

CHAPTER 1

Introduction

1.1 Introduction

Titanium is a chemical element in the periodic table having the symbol Ti, atomic number 22, and atomic weight 47.90. It occurs in the fourth group of the periodic table, and its chemistry shows similarities to that of silicon and zirconium. The outer electronic arrangement is $3d^24s^2$, and the principal valence state, correspondingly of 4+, 3+ and 2+, is also known as being less stable. The element burns in air when heated to give the oxide, TiO_2 . Titanium occurs in nature as ilmenite ($FeTiO_3$), rutile (tetragonal TiO_2), anatase (tetragonal TiO_2), brookite (rhombohedral TiO_2), perovskite ($CaTiO_3$), sphene ($CaTiSiO_5$), and geikielite ($MgTiO_3$) (Kirk and Othmer, 1985 : 1182).

Titanium is well known for its excellent corrosion resistance (almost as resistant as platinum), being able to withstand attack by acid, moist chlorine gas, and common salt solutions. Pure titanium is not soluble in water but soluble in concentrated acids. It is a light strong metal with low density (40% as dense as steel) that, when pure, is quite ductile (especially in an oxygen-free environment), easy to work, lustrous, and metallic-white in color. The relatively high melting point of this element makes it useful as a refractory metal. Titanium is as strong as steel, but 45% lighter, 60% heavier than aluminium, and twice stronger. These properties make it very resistant to the usual kinds of metal fatigue. Some of its properties are given in Table 1.

Approximately 95% of titanium is consumed in the form of titanium dioxide (TiO_2), an intensely white permanent pigment with good covering power in paints, paper, and plastics. Paints made with titanium dioxide are excellent reflectors of infrared radiation and are used in exterior paints. It is also used as a strengthening filler in paper and cement. Because of high tensile strength (even at high temperatures), light weight, extraordinary corrosion resistance, and ability to withstand extreme temperatures, titanium alloys are principally used in aircraft, armor painting, naval ships, spacecraft and missiles. It is used in steel alloys to reduce grain size and as a deoxidizer but in stainless steel it is employed to reduce carbon content. Titanium is often alloyed with aluminium (to refine grain size), vanadium, copper (to harden), iron, manganese, molybdenum, and with other metals (<http://en.wikipedia.org/wiki/Titanium>).

Table 1 Properties of titanium

Property	value
^a Electronic structure	3d ² 4s ²
^b Melting point, °C	1668 ± 5
^b Boiling point, °C	3260
^b Density, g/cm ³	
α phase at 20 °C	4.507
β phase at 885 °C	4.35
^b Thermal conductivity at 25 °C, W/(m·K)	21.9
^b Electrical resistivity at 20 °C, nΩ·m	420
^b Magnetic susceptibility, mks	180 x 10 ⁻⁶
^b Modulus of elasticity, Gpa	
tension	ca. 101
compression	103
shear	44
^a Metallic radius (Å)	1.47
^a Entropy S ₂₉₈ (cal/deg/mol)	7.33
^a E (M ²⁺ /M) volts, 25 °C	-1.63
^a E (M ³⁺ /M ²⁺) volts, 25 °C	-0.37
^a Heat of atomisation (kcal/g·atom)	112.6

a (Clark , 1968 : 6), b (Kirk and Othmer ,1985 : 1183)

Titanium dioxide occurs primarily in three different forms: anatase, brookite, and rutile. The most common are anatase and rutile, since brookite is rather unstable. The brookite type cannot be used in industries because of its instability at room temperature. The anatase type has the problems of poor light, heat resistance, and gradually decreasing in whiteness due to weather. It also has drawbacks for applications involving adsorption technology owing to its low surface energy. The rutile type has outdoor applicability because of its good light resistance and can be applied to surfaces by the use of adsorption technology without advanced skills or sophisticated equipment (Kim and Chung, 2001).

In recent years, titanium dioxide photocatalysis has been studied extensively as a potential technique for the treatment of pollutants (both organic and inorganic) and microorganisms. Among these polymorphs, TiO_2 in the anatase structure has been used as an excellent photocatalyst for photodecomposition and solar energy conversion due to its high photoactivity. Generally, anatase has higher photocatalytic activity than rutile. However, the mixed phase of anatase and rutile has higher photoactivity than pure anatase or rutile phase.

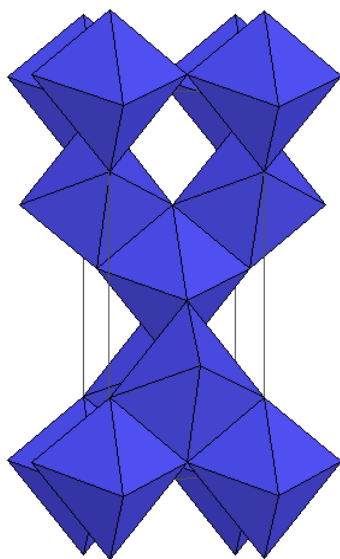
The photocatalytic performance of rutile is desired to increase in an attempt to use it in a room illuminated by fluorescent light or incandescent lamp. The rutile-type titania is expected to be suitable for such application due to its lower optical band gap energy (3.0 eV), and less photocatalytic efficiency compared to the anatase due to the less recombination probability of activated electron and hole under solar light. Therefore, in the modification of the rutile by metal ion doping was concentrated in this study our attention in improve its photocatalytic efficiency. The aims of this research are; (a) to find a lower temperature method for synthesis of rutile phase (undoped TiO_2) and metal doped rutile TiO_2 and compare some properties to the undoped TiO_2 , (b) to examine the effect of dopants on the photocatalytic degradation of methylene blue (MB) dye in the aqueous suspensions of synthesized TiO_2 under UV light irradiation.

1.2 Review of Literatures

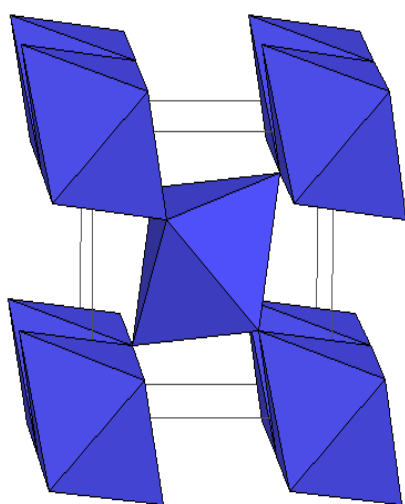
Titanium dioxide is a polymorphic compound, having three polymorphous structures: anatase, brookite, and rutile. These polymorphic forms of titanium dioxide are shown in Figure 1. Crystallographic data on the three oxide modifications are summarised in Table 2. Both anatase and rutile are tetragonal, whereas brookite is orthorhombic. In all three oxide modifications, each titanium atom is coordinated to six almost equidistant oxygen atoms, and each oxygen atom to three titanium atoms (Clark, 1968 : 269). In the case of anatase, the TiO_6 octahedron is slightly distorted, with two Ti-O bonds slightly greater than the other four, and with some of the O-Ti-O bond angles deviating from 90° . The distortion is greater in anatase than rutile. The structure of anatase and rutile crystals have been described frequently in terms of chains of TiO_6 octahedra having common edges. Two or four edges are shared in rutile and anatase, respectively. The third form of titanium dioxide, brookite, the interatomic distances and the O-Ti-O bond angles are similar to those of rutile and anatase. The essential difference is that there are six different Ti-O bonds

ranging from 1.87 to 2.04 Å. Accordingly, there are 12 different O-Ti-O bond angles ranging from 77° to 105° . Brookite are formed by joining together the distorted TiO_6 octahedra sharing three edges. All three oxide modifications are birefringent ; anatase is uniaxial negative, brookite is biaxial positive and rutile is uniaxial positive. Further data are given in Table 3.

(a) Anatase



(b) Rutile



(c) Brookite

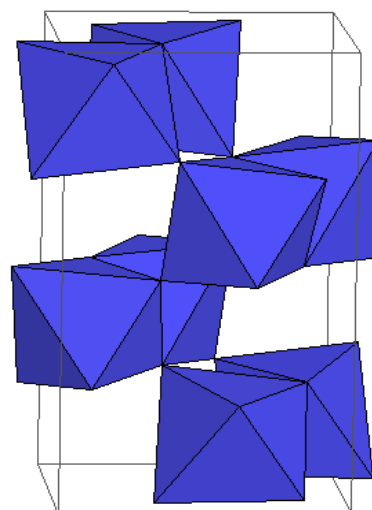


Figure 1 Crystal structure of TiO_2 ; (a) Anatase, (b) Rutile, and (c) Brookite

Table 2 X-ray data on TiO₂ modifications (Clark ,1968 : 268).

	Space group	Z	Cell parameters (Å)			Ti-O (Å) ^b
			A	B	C	
Anatase	$C_{4h}^{19} = C4/amc$	8	5.36		9.53	1.91(2) 1.95(4)
Brookite	$D_{2h}^{15} = Pbca$	8	9.15	5.44	5.14	1.84-2.03
Rutile	$D_{4h}^{14} = P4_2/mnm$	2	4.954		2.959	1.944(4) 1.988(2)
α - PbO ₂ form	$D_{2h}^{14} = Pbcn$	4	4.515	5.497	4.939	1.91(4) 2.05(2)

^b The numbers in parentheses refer to the number of equivalent oxygen atoms at the stated distance from a titanium atom.

In industry, it is well known that TiO₂ pigments are produced by the older sulfate or newer chloride processes. The economics of the two processes are very much dependent upon the raw material available. The starting materials for TiO₂ production are ilmenite and titaniferous slag in the case of the sulfate process (Figure 2) and leucoxene, rutile, synthetic rutile, and in the future possibly also anatase, for the chloride process (Figure 3) (Büchner, et al., 1989 : 523-525).

Table 3 Properties of the three modifications of titanium dioxide (Clark, 1968 : 270).

	<i>Anatase</i>	<i>Brookite</i>	<i>Rutile</i>
Density (g/cc)	3.90	4.13	4.27
Hardness (Mohs's scale)	5.5-6.0	5.5-6.0	6.0-6.5
Melting Point (°C)	change to rutile	change to rutile	1840 ± 10
Entropy $S_{298.16}^{\circ}$ (cal/deg/m)	11.93	-	12.01
Refractive Index (25 °C) ($\lambda = 5893 \text{ \AA}$)	n_{ω} 2.5612 n_{ϵ} 2.4880	n_{α} 2.5831 n_{β} 2.5843 n_{γ} 2.7004	n_{ω} 2.6124 n_{ϵ} 2.8993
Dielectric Constant	$\epsilon = 48$ (powder)	$\epsilon = 78$	$\epsilon_{av} \approx 110$ $\epsilon_{II} = 180$ at $3 \times 10^5 \text{ c/s}$ 25 °C $\epsilon_{\perp} = 89$, at $3 \times 10^5 \text{ c/s}$ 25 °C

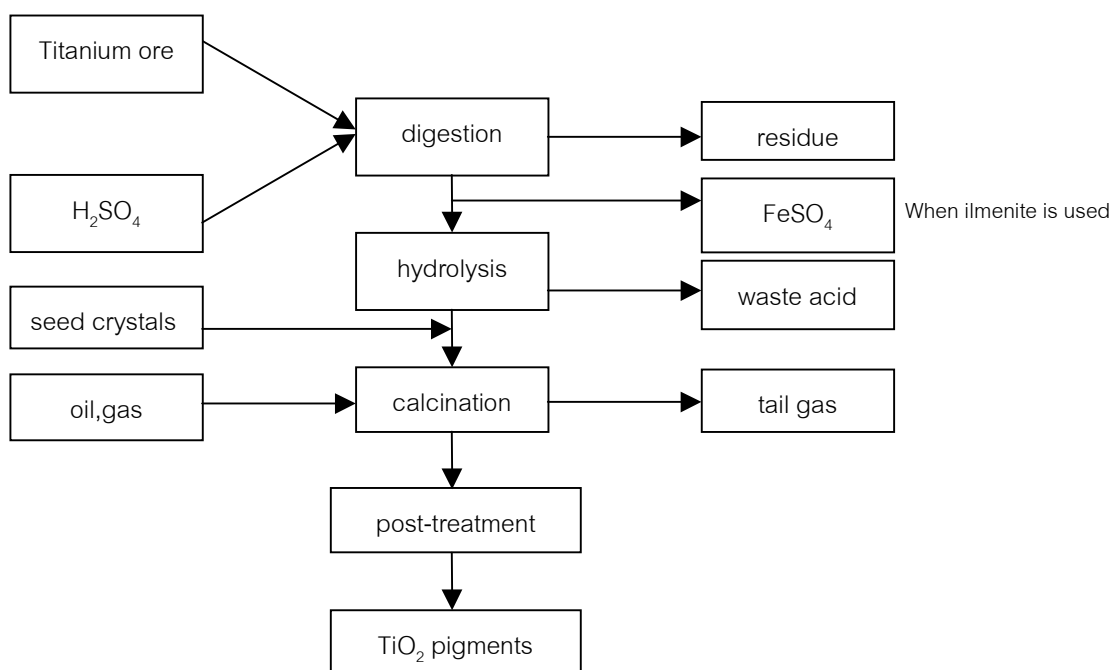


Figure 2 TiO₂ pigment manufactured by the sulfate process

(Büchner, et al.,1989 : 526).

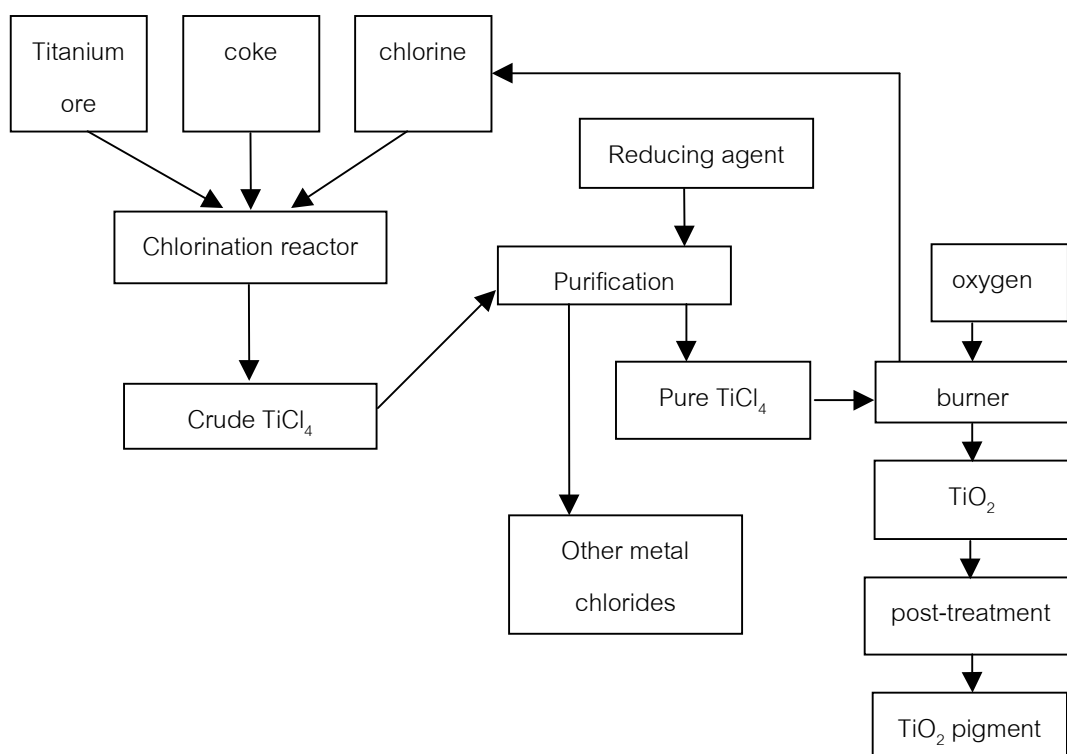


Figure 3 TiO₂ pigment manufactured by the chloride process

(Büchner, et al.,1989 : 528).

The sulfate process was the first commercial scale technology used to convert ilmenite to TiO_2 . The process started from digestion the finely ground raw materials in an exothermic reaction with concentrated sulfuric acid, the digested cake dissolved in cold water and the residue separated off. To prevent their precipitation during the subsequent hydrolysis the Fe(III) ions are reduced to Fe(II) by adding a Ti(III) solution or scrap-ions. Upon evaporation of the solution, the large quantities of iron(II) sulfate heptahydrate is produced, when ilmenite is used, and crystallize out. The titanium oxysulfate is then hydrolyzed to titanium oxyhydrate by heating the clear solution with steam at 95-110°C. TiO_2 seed crystals are added or formed before hydrolysis to ensure yields of 93-96 % TiO_2 and to obtain a hydrolysis product which yields the optimum particle size of ca. 0.2 μm upon firing. Diluted sulfuric acid remains as “waste acid”. The hydrolysis product is washed, treated with a Ti(III) solution to remove adsorbed heavy metal ions (Fe, Cr, Mn, V) and calcined at temperature between 800-1,000°C. Anatase or rutile pigments can be produced in the calcination process depending upon the choice of additives, which determine the characteristics of the product. TiO_2 obtained in this way usually has the structure of anatase since the sulfate ions stabilize this modification (Hadjiivanov, et al., 1996) which could not be removed during the process of washing, and it would benefit to the formation of anatase and the transformation temperature must take place at high temperature (about 1,000°C) to obtain rutile TiO_2 (Yang, et al., 2002).

The newer chloride process offers tighter product control, less labor intensive, avoids the iron sulfate waste problem and, at larger scales, is cheaper to operate. Currently about 60 % of 4 million tones of pigment produced world-wide is produced by this process. This process required the ilmenite to be processed to the rutile form (i.e. removal of the iron component to yield crude titanium dioxide(synthetic rutile)). The chloride process started from the reaction of chlorine with synthetic rutile to form raw titanium tetrachloride which is then mixed with reducing agent to convert impurities such as vanadium oxychloride, iron chloride to lower oxidation state compounds. It is then distilled yielding titanium tetrachloride in almost any required purity. Finally, it is combusted with pure oxygen to TiO_2 and chlorine, which is reused in the chlorination. Usually, TiO_2 prepared from this process has the mixture structure of anatase and rutile with the average diameter about 20 nm. For instance, the typical commercial formed TiO_2 (anatase) made by Degussa contain about 25 % rutile.

On a laboratory scale, titanium dioxide has been prepared by various methods, such as sol-gel method, hydrothermal method, combustion synthesis, inert-gas conversion and so on. The different preparation route and the experiment conditions of titanium dioxide result in products with different structures, morphology, particle size, and contaminants (Hadjiivanov, et al., 1996). The metal alkoxide is usually used as a precursor on a laboratory scale to prepare titanium dioxide powders. However, strict control of the reaction conditions is required because of the intense hydrolysis of alkoxide in the air and the prices of the alkoxide limit the commercialization. So, the commercial inorganic compounds such as titanium tetrachloride (TiCl_4) and titanium disulfate ($\text{Ti}(\text{SO}_4)_2$) are more extensively used in the preparation of titanium dioxide than the metal alkoxide.

For the past decade, the sol-gel technique has been used in many applications in science and technology such as membranes, porous substrate, photocatalytic oxides, ceramics, glass materials and also in electronic devices (Kumar, et al., 1998). In general, the sol-gel process involves the evolution of inorganic networks through the formation of a colloidal suspension (sol) and gelation of the sol form a network in a continuous liquid phase (gel). An overview of the sol-gel product is presented in Figure 4.

The starting materials in the preparation of the “sol” are usually inorganic metal salts or metal organic compounds as a metal alkoxide. In a typical sol-gel method, the precursor is subjected to a series of hydrolysis and polymerization (condensation) reactions to form a colloidal suspension or a “sol”. Further processing of the “sol” enables one to make ceramic materials in different forms. Thin films can be prepared on a piece of substrate by spin coating or dip-coating. When the “sol” is cast into a mold, a wet “gel” will form. With further drying and heat-treatment, the “gel” is converted into dense ceramic or glass articles. If the liquid in a wet “gel” is removed under a supercritical condition, a highly porous and extremely low density material called “aerogel” is obtained. As the viscosity of a “sol” is adjusted into a proper viscosity range, ceramic fibers can be drawn from the “sol”. Ultra-fine and uniform ceramic powders are formed by precipitation, spray pyrolysis, or emulsion techniques (Chemat Technology, Inc., 1998).

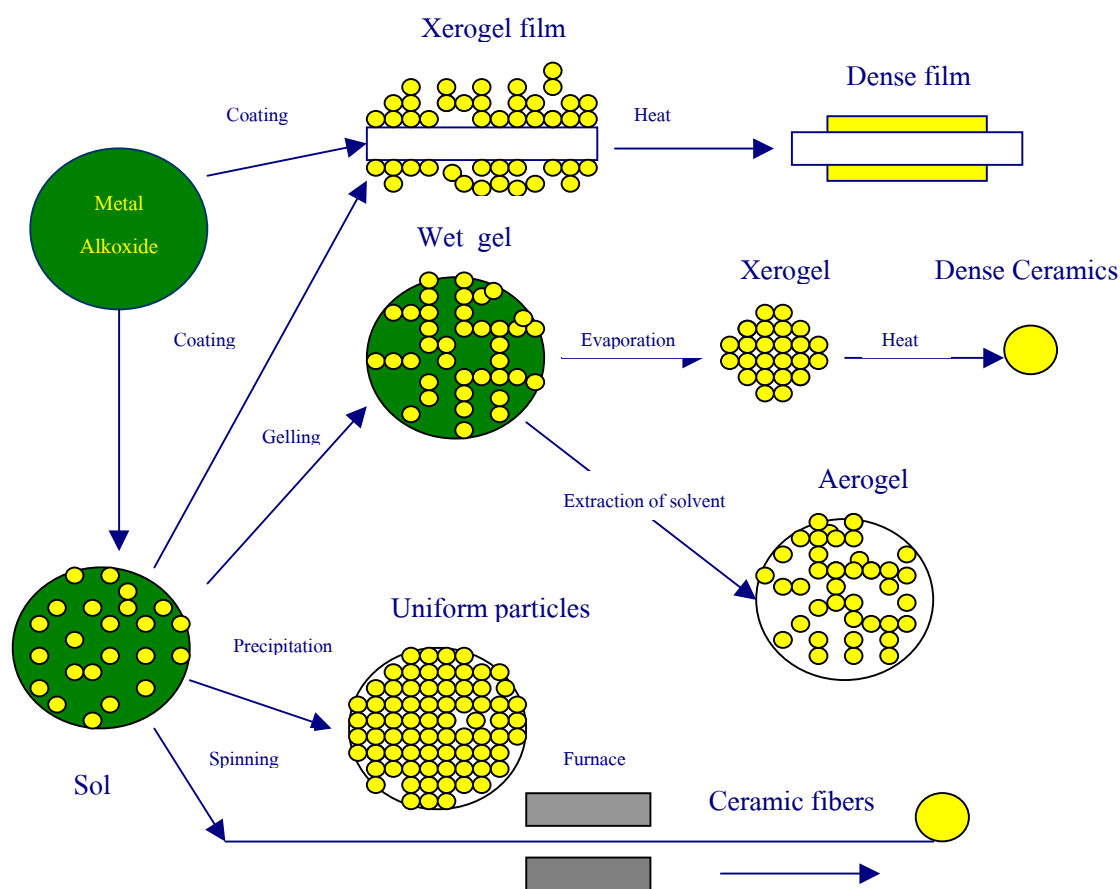


Figure 4 An overview of products prepared by sol-gel methods
(Chemmat Technology, Inc., 1998)

In comparison to the other methods, the sol-gel method offers many advantages such as easy control, accessibility of nanocrystalline materials, homogeneous multicomponent oxides obtain a large amount of TiO_2 powders with high photocatalytic activity and chemical purity (Suresh, et al., 1998). Moreover, in these method precursor materials are metallic halide or alkoxide that favor the building of a solid network in a gel which eventually become a stable solid (Sanchez, et al., 1996). When this method is used for developing catalytic materials, it provides very interesting results. For instance, in metal supported catalysis, the active metal and the support can be prepared in one step. This allows an economy in the catalyst preparation, and also allows one to develop catalyst with new properties (Bokhimi, et al., 1995). Furthermore, the sol-gel method can be used for preparing the support alone, these supports determine the dispersion and stabilization of the active metal and has a specific surface area that can be regulated by controlling its particle size

and porosity (Tauter, et al., 1978). Many studies have shown that titanium dioxide powder obtained from sol-gel method has a good properties for application as follows.

Anderson, et al., (1995) studied the effect of incorporation of SiO_2 on TiO_2 -based photocatalyst prepared by sol-gel method. They also investigated the photodecomposition of rhodamine-6G (R-6G). The powders prepared from the reaction of tetraisopropyl orthotitanate (TIOT) and tetraethoxysilane (TEOS). A mixture TIOT/TEOS with the desired Ti/Si ratio was prepared in a dry box, sealed, and then removed from the drybox. This solution was added dropwise to a solution of 250 mL anhydrous 2-propanol and 1 mL of concentrated HCl at 0°C with vigorous stirring. The mixture was allowed to age at room temperature in a covered beaker for 1 week after gelling. Solvent was then removed under vacuum, and while still under vacuum, the catalysts were heated to 200°C for 12 h. The resulting glassy materials was ground in a mixture mill for 1 h. The products determined by XRD, BET surface area and UV-VIS techniques. Application of photocatalysts with different $\text{SiO}_2/\text{TiO}_2$ ratio to the photodecomposition of R-6G demonstrates that a ratio of 30/70 shows more efficient photocatalyst about 3 times for the destruction of R-6G than Degussa P25 TiO_2 . The presence of an adsorbent (SiO_2) promoted efficiency by increasing the quantity of R-6G near the TiO_2 sites relative to the solution concentration of R-6G. Photogenerated oxidants from TiO_2 had been shown to be mobile either in solution or on the surface of SiO_2 .

Sanchez, et al., (1995) synthesized TiO_2 and Pt/TiO_2 materials at pH 3 and 9 by sol-gel process using titanium alkoxide as reactant. The reactant was added drop by drop into the mixture of distilled water, HCl, and absolute ethanol. Then this mixed solution was refluxed at 70°C with constant stirring and adjust pH of solution (pH = 3, 9). The reflux was maintained until the gel was formed. These samples were dried at 70°C for 24 h and these reactant gels were calcined in air for 24 h at 200, 400, 600, 800°C . The resultant solids were studied by UV-Vis diffused reflectance spectroscopy. The calculation of band gap energy using UV-Vis technique is an indirect method for determining the semiconductive and photoconductive properties of TiO_2 . It is proposed that the formation of vacancies in titania samples prepared at pH 3 is due to the dehydroxylation of the sample and subsequent dehydration. On the other hand, when the samples are prepared at pH 9 the formation of vacancies is due to a surface oxygen desorption phenomenon. In the Pt/TiO_2 samples

the reduction of platinum during dehydroxylation process occurs and the reduced platinum acts as an electron trap.

Haddow, et al., (1996) prepared thin film titania by sol-gel method. The titania film was prepared by hydrolysis of starting sol (titanium(IV) isopropoxide and 50 mL of isopropanol), a chelating agent, diethanolamine. In this study, a small amount of water (0.8 mL) was added to the solution of alkoxide to partially polymerize the Ti species. The whole solution was kept in air-tight container and stirred magnetically for 24 h. Microscope coverslips was cleaned ultrasonically and washed with distilled water and acetone prior to dip coating in laminar air flow cabinet. These slips were fired for period of 1 or 3 h in air furnace at temperatures between 373 and 873 K. In this work, they also have investigated the effect of dip rate, sintering temperature and time on the chemical composition of the films, their physical structure and thickness, and adherence to a silica substrate. These thin surface films of titania have been deposited onto glass substrates. The use of low doping rate prevents cracking in this films, irrespective of the subsequent firing time or temperature. Firing at higher temperature (873 K) produces predominantly glass films and these mimic closely in chemistry the natural oxide layer that is formed on Ti implants. Lower firing temperature produce films that retain a high content of organic component and water. However, even at the lowest dip rate employed, the films produced are two orders of magnitude thicker than the natural Ti oxide layer. Refinement of the dipping set-up, or the use of dilute solution, may result in the production of thinner films. Thinner films will almost certainly be crack-free after firing and may result in less organic products being trapped in the film during the firing process. The usage of these films are intention to develop an in vitro model to study the phenomenon of osseointegration. These films provide surfaces that are easily formed, and that may be chemically altered by the addition of salts to the sol. Coatings may be deposited onto a wide range of materials, offering the exciting possibility of removal of the coating at a later stage: this would be particularly beneficial, enabling the study of osseointegration by TEM and photon-based spectroscopies.

Marci, et al., (1996) prepared tungsten oxide/ TiO₂ polycrystalline samples (W/Ti) by the sol-gel method. The mixed propan-2-ol solutions of tungsten and titanium alkoxides were stirred and suddenly form a yellow suspension for 1 h. Then it was heated to reflux for 5 h giving a transparent pale-green solution. Different volumes of tungsten precursor solution (1.3, 2.6, 12.8,

25.7 and 51.4 mL) were added to the titanium alkoxide solutions to obtain the desired W/Ti molecular ratios. All these solutions, together with a solution of titanium alkoxide without tungsten, used for obtaining the precursor of pure TiO_2 , were hydrolysed by adding hydrochloric acid solution diluted in 10 mL of propan-2-ol. The resulting almost colorless solutions were stirred at room temperature for 24 h and aged in open vessels. Gelation occurred after 2-3 days yielding pale-yellow gels. The gels were dried under reduced pressure for 7 days and then were ground and sieved, collecting a powder fraction with particle sizes $< 200 \mu\text{m}$. The powders obtained in this way were crystallised by heat treatment at 823 K for 15 h. After crystallisation, the samples appeared to be different colours. The powders changed from pale yellow to pale blue as the W:Ti ratio decreased, whereas the pure TiO_2 sample was white. These products have been characterized using several techniques, namely thermogravimetric analysis, gas-chromatography, mass spectroscopy or with gas chromatography/mass spectrometry, X-ray diffraction, X-ray photoelectron spectroscopy, determination of specific surface area, scanning electron microscopy, Fourier-transform infrared spectroscopy and monitoring of pyridine adsorption for surface acidity. Moreover the tungsten oxide/ TiO_2 samples have been employed as catalysts for 4-nitrophenol photodegradation in aqueous suspensions used as a probe reaction. The results indicate that the surface of the W/Ti particle is enriched with homogeneously dispersed tungsten as well as microcrystalline or amorphous species. A tentative explanation for the photocatalytic behaviour of the samples has been provided, taking into account both the formation of surface layers of tungsten species. It has been hypothesised that octahedrally co-ordinated tungsten oxide species are produced on the particle surface and some heterojunctions along with the interface acceptor states, could improve the separation of the photoproduced pairs and, consequently, could be responsible for the observed higher photoreactivity. The maximum photoactivity for 4-nitrophenol photodegradation was achieved for a sample containing 1.7 molW per 100 mol Ti.

Anderson, et al., (1997) prepared mixed oxides of $\text{TiO}_2/\text{SiO}_2$ and $\text{TiO}_2/\text{Al}_2\text{O}_3$ by sol-gel method and studied the photocatalytic decomposition of phenol and salicylic acid in an air-saturated aqueous solution. The $\text{TiO}_2/\text{SiO}_2$ was prepared by the same method as given in their earlier report (Anderson, et al., 1995). The $\text{TiO}_2/\text{Al}_2\text{O}_3$ was prepared from the reaction of tetraisopropyl orthotitanate (TIOT) and triisopropyl orthoaluminate (TIOA). A solution of 20 g TIOA in 500 mL of 2-propanol was prepared and stirred for 8 h. The solution was cooled to 0°C and TIOT was

added dropwise with stirring for 1 h. The resulting solution was slowly warmed to room temperature and stirred for 8 h. The mixture was allowed to age in the liquor for 7 days. After aging the solvent was removed under vacuum at room temperature. The dry powder was then heated and used as a photocatalyst. It was found that $\text{TiO}_2/\text{Al}_2\text{O}_3$ material showed more activity for the photocatalytic decomposition of salicylic acid than $\text{TiO}_2/\text{SiO}_2$ and TiO_2 -only materials. $\text{TiO}_2/\text{SiO}_2$ materials showed more activity for the photocatalytic decomposition of phenol when compared to the other materials. The increasing in efficiency was attributed to the presence of matrix-isolated TiO_2 quantum particles in the $\text{TiO}_2/\text{SiO}_2$ which promote the adsorption of phenol and a higher decomposition rate than $\text{TiO}_2/\text{Al}_2\text{O}_3$ and pure TiO_2 . While the $\text{TiO}_2/\text{Al}_2\text{O}_3$ materials behave more as a composite of the two bulk phases which adsorbed acidic species and showed more efficiency in photocatalytic decomposition of salicylic acid.

Yang, et al., (1998) studied the effect of three levels of zirconia (ZrO_2) additive on the anatase-rutile transition. Titania powders with or without zirconia additive were prepared by sol-gel processing. The mixed solution of titanium isopropoxide ($\text{Ti}(\text{OPr})_4$) and zirconium oxychloride ($\text{ZrOCl}_2 \cdot 8\text{H}_2\text{O}$) were then mixed in different portions according to Zr/Ti molar ratios of 0, 0.05, 0.075, and 0.10. All mixed solutions were adjusted to a constant pH value of 1.5 by 3N HNO_3 . Hydrolysis was carried out by adding distilled water ($\text{H}_2\text{O}/\text{Ti} = 2$) to the mixed solutions. The final concentration of Ti precursor was fixed at 0.33 M for all cases. The obtained gels were held at room temperature for 2 days and then dried in an oven at 50 °C and 120 °C for one day at each temperature. The as-prepared xerogels were ground and then calcined at temperatures of 600, 900, and 1200 °C for 1 h at a heating rate of 5 °C/min. The synthesized powder was investigated using differential thermal analysis and X-ray diffraction. The ZrO_2 additive was found to retard the anatase-rutile transition. The formation of a limited solid solution of ZrO_2 in TiO_2 (solubility less than $\text{Zr}/\text{Ti} = 0.075$) at relatively low temperature, which probably increases the strain energy of TiO_2 particle, is responsible for the increased transition temperatures. The apparent activation energy of anatase-rutile transition in the presence of ZrO_2 additive ($\text{Zr}/\text{Ti} = 0.05$) was determined as 468 kJ/mol.

Suresh, et al., (1998) prepared titanium dioxide powders by sol-gel method with acetic acid as a modifier at different pH conditions. The phase transformation during heat treatment

was investigated by impedance spectroscopic measurements and the data were compared with those obtained from thermal analysis and XRD techniques. The samples were prepared by hydrolysis of 25 mL titanium isopropoxide dissolved in 48 mL acetic acid and was stirred for 0.5 h. To this solution 150 mL double distilled water was added dropwise under continuous stirring for 1 h. The pH was adjusted to 3 by adding 10 % ammonium hydroxide. The mixture was heat to 70°C in an air oven to get a gel. Similar procedures were followed to prepare titanium dioxide samples at pH values 4, 5 and 6. The studies showed that the anatase to rutile phase transformation was delayed in the case of acetic acid modified gel precursor at pH 3 and 4, showing the presence of anatase phase even at 1,000°C. On the other hand, in the sample precursor prepared at pH 6, anatase to rutile transformation was complete at 800°C, under identical conditions of heat-treatment.

Wang, et al., (1999) synthesized various metal-doped TiO₂ nanoparticles with sol-gel method. For undoped TiO₂ were prepared from hydrolysis of titanium tetrabutanoxide (Ti(OBu)₄). The solution of Ti(OBu)₄ was added dropwise under vigorous stirring to 45 mL of distilled water which was adjusted to pH 1.5 with nitric acid. The resulting colloidal suspension was heated at 65 °C for 2 h to obtain a transparent colloidal suspension of TiO₂. Doped TiO₂ samples were prepared according to the above procedure in the presence of added metal salts to give a doping level of 0.5 mol%. Metal salts used as precursor for dopant ions are listed as follows: La(NO₃)₃, Nd(NO₃)₃, Pr(NO₃)₃, Sm(NO₃)₃, Eu(NO₃)₃, Zn(NO₃)₂, Cd(NO₃)₂, Fe(NO₃)₃, Cr(NO₃)₃, and Co(NO₃)₂. These precursors were dissolved in distilled water (pH 1.5). These products were characterized with TEM and XRD. The related electrodes were also prepared and their photoelectrochemical properties were studied. The charge of photocurrent with the electrode potentials and the wavelengths of incident light showed two different characteristics for metal-doped TiO₂ electrodes. For Fe³⁺-doped TiO₂ electrode, the characteristic of p-n photoresponse coexistence was observed, while for other metal-ion (such as La³⁺, Nd³⁺, Pr³⁺, Sm³⁺, Eu³⁺, Zn²⁺, Cd²⁺ and Co²⁺-doped TiO₂ electrode, the characteristic of n-type semiconductor was observed. The effect of the content of Zn²⁺ on the photocurrent was investigated and the result showed that the incident photon conversion of Zn²⁺ was 0.5% which was due to that there is an optimal doping concentration for Zn²⁺ ion to make the thickness of the space charge layer to be about the same as the penetration depth of light.

Escobar, et al., (2000) prepared Al_2O_3 - TiO_2 materials by the sol-gel method using aluminium tri-*sec*-butoxide and titanium (IV) isopropoxide as precursors with different synthesis additives: HNO_3 , NH_4OH , and CH_3COOH . The materials at two compositions: Al/Ti atomic ratio = 2 and 25 were synthesized at 278 K and calcined at temperature from 573 to 1173 K. These solids were characterized by TGA, DTA, XRD, BET and SEM. The complexing (CH_3COOH) and the basic (NH_4OH) additives led to solids with high pore volumes and broad pore size distributions. On the one hand, very high surface area: $525 \text{ m}^2/\text{g}$ for solids calcined at 773 K was found for samples prepared with CH_3COOH . On the other hand, high temperature stability was obtained with NH_4OH addition ($200 \text{ m}^2/\text{g}$, for Al_2O_3 -rich samples at 1173 K). HNO_3 catalyzed samples showed lower surface areas and pore volumes. Surface areas and sintering behavior were a function of titanium dioxide content. TiO_2 -rich samples showed higher surface area (773 K) than Al_2O_3 -rich samples, but at more severe conditions they suffered a severe specific area loss. The Al_2O_3 -rich formulations showed good stability in the whole range of temperature studied.

Harizonov, et al., (2001) studied the mixed oxide system TiO_2/MnO prepared by the sol-gel method using titanium ethoxide and manganese nitrate as precursors. The xerogels of the solutions dried at 80°C and treated at 560°C in air for 1 h and then characterized by XRD, FT-IR, DTA and UV-VIS techniques. The results showed that the sol-gel method could be used to prepare good quality nanocrystalline TiO_2 coatings. In addition, the presence of MnO in TiO_2 xerogels was effective in decreasing the anatase-rutile transformation temperature. These coatings offered prospective applications in passive solar control glazing due to the relatively high refractive index.

Khalil, et al., (2001) prepared ceramic powder in the system SiO_2 - TiO_2 - Al_2O_3 by sol-gel technique. Aluminum trisecbutylate ($\text{AlO}_3\text{C}_{12}\text{H}_{27}$), titanium isopropoxide ($\text{TiO}_4\text{C}_{14}\text{H}_{28}$) and tetraethylorthosilicate ($\text{SiO}_4\text{C}_8\text{H}_{20}$)(TEOS) were used as precursors. The alkoxides in the required proportions were dissolved in isopropyl alcohol. The alkoxide solution was then hydrolyzed using a mixture of alcohol, distilled water and 0.5 mol HCl. The produced gel was then dried stepwise between 60°C and 120°C for 24 h. The obtained powders were then calcined at 800°C during 3 h. The products were studied through nitrogen gas adsorption at liquid nitrogen temperature and application of the Brunauer-Emmett-Teller (BET) equation. The results of investigated sol-gel powders shown the different types of pores present in the samples. The influence of thermal

treatment (drying, calcination) on the surface characteristics of the investigated powder shown that surface area decreased after calcination at 800 °C.

Li, et al., (2001) prepared photocatalyst ($\text{WO}_x\text{-TiO}_2$) powder by sol-gel method. A 0.05 mol TiO_2 transparent sol was first prepared using $\text{Ti}(\text{OBU})_4$, 120 mL absolute ethanol, 15 mL acetic acid, and 5 mL distilled water, and aged for 1 day. Then 3.0 mL aqueous solution of ammonium tungstate $(\text{NH}_4)_{10}\text{H}_2\text{W}_{12}\text{O}_{42}\cdot 4\text{H}_2\text{O}$ was added dropwise to the sol under vigorous stirring for 2 h until $\text{WO}_x\text{-TiO}_2$ gel formed. $\text{WO}_x\text{-TiO}_2$ sample was obtained in a doping level of 1.5% after aged, dried, ground and sintered at 973 K for 2 h. The photooxidation efficiency of $\text{WO}_x\text{-TiO}_2$ catalyst was also evaluated by conducting a set of experiments to photodegrade methylene blue (MB) in aqueous solution. The photocatalytic activity of $\text{WO}_x\text{-TiO}_2$ was examined by XRD, UV-Vis absorption spectra, XPS, photoluminescence spectra (PL), surface photovoltage spectra (SPS) and electron-field-induced surface photovoltage spectra (EFISPS). The experiments demonstrated that the MB in aqueous solution was successfully photodegraded using $\text{WO}_x\text{-TiO}_2$ under visible light irradiation. It was found that an optimal WO_x dosage of 3% in $\text{WO}_x\text{-TiO}_2$ achieved the highest rate of MB photodegradation in this experimental condition. It has been confirmed that $\text{WO}_x\text{-TiO}_2$ could be excited by visible light ($E < 3.2$ eV) and the recombination rate of electrons/holes in $\text{WO}_x\text{-TiO}_2$ declined due to the existence of WO_x doped in TiO_2 . The order of its photoactivity from weak to strong had good agreement with that of PL intensity and that of EFISPS intensity from strong to weak.

Zhang, et al., (2001) prepared nanocrystalline iron doped titanium dioxide as a single-phase product by sol-gel method. The product synthesized from the reaction of titanium isopropoxide and $\text{Fe}(\text{NO}_3)_3\cdot 9\text{H}_2\text{O}$ by varying the iron dopant amounts: 0, 1, 2, 3, 4, 5 and 6 atom %. The mixture was aged at ambient temperature for a few days. During this time liquid became progressively more viscous and eventually a dry gel formed. Crystallization was achieved by subsequent calcination of the dry gel in air at different temperatures. By transmission, scanning, and analytical electron microscopy as well as by complementary techniques it has been found that the as-prepared solids exhibit a narrow size distribution and that the iron is homogeneously distributed in the titanium dioxide matrix. The influence of the iron concentration on the phase transformations of the doped titanium dioxide was investigated by X-ray diffractometer. The formation of the iron

titanium dioxide pseudobrookite, $\text{Fe}_2\text{Ti}_2\text{O}_5$, was observed above 670°C , but only for an iron content of more than 3 atom %. UV-spectroscopic measurement revealed that the absorption spectrum of the iron doped titanium dioxide is sensitively related to both the iron concentration and the calcination temperature. Whereas pure nanocrystalline titanium dioxide undergoes grain growth (sintering) when the calcination temperature is increased, iron doped titanium dioxide proves to be inert to grain growth, N_2 adsorption-desorption analysis indicated that the products calcined between 390 and 600°C for 1 h in air have mesoporous structure and the distribution of mesopores is very narrowly, centered at 3.7 nm.

Arroyo, et al., (2002) studied the anatase-rutile phase transformation of TiO_2 containing various amount of Mn^{2+} ions which prepared by sol-gel process from titanium(IV) isopropoxide and manganese (II) acetate tetrahydrate. The mixture was stirred at room temperature for 20 min. After that, 3 mol of deionized water were added, and major precipitation occurs. The stirring was continued for another 60 min. The resultant mixture was aged for 72 h, and xerogels were obtained by heating at 80°C for 72 h. The amorphous powders were calcined for 2 h at different temperatures. Significant structural changes were observed during the various stage of the phase transformation. It is shown that at low dopant concentrations, manganese ions are incorporated in the TiO_2 structure, and the anatase phase is stabilized, but at larger amounts, part of the dopant is segregated on the surface of TiO_2 and the rutile formation is accelerated. An increase in treatment temperature oxidized Mn^{2+} to Mn^{4+} . The dopant ions favor the nucleation of rutile in the surface and spread out their growth into TiO_2 particles, lowering the anatase-rutile transformation temperature.

Yang, et al., (2002) prepared nanoparticles of TiO_2 co-doped with Fe^{3+} and Eu^{3+} using sol-gel method. In a typical experiment, $\text{Ti}(\text{O}i\text{Bu})_4$ was added dropwise to distilled water adjusted to pH1.5 with nitric acid under vigorous stirring at room temperature. Then, the temperature was raised to 60°C and kept 6 h for better crystallization of nano- TiO_2 particles. The resulting translucent colloidal suspension was evaporated using a rotary evaporator. The obtained powder was washed with isopropanol and dried at 50°C until complete evaporation of the solvent. Doped and co-doped TiO_2 particles were synthesized using almost the same method. The appropriate amount of $\text{Fe}(\text{NO}_3)_3 \cdot 9\text{H}_2\text{O}$ and/or Eu_2O_3 dissolved in 1 M HNO_3 was added to distilled

water prior to the hydrolysis of $\text{Ti}(\text{OBU})_4$. The remaining procedures were the same as described above. The photocatalytic reactivities were evaluated by photodegradation of chloroform in solution. Nanocrystalline TiO_2 co-doped with Fe^{3+} and Eu^{3+} at optimal concentration (1 at.% Fe^{3+} , 0.5 at.% Eu^{3+}) shows a synergistic effect, which significantly increase the photodegradation activity of nano- TiO_2 . The effect of the dopants of Fe^{3+} and Eu^{3+} in TiO_2 play different roles in improving the photoinduced charge separation in the nanostructured semiconductor in the interfacial charge transfer process at the semiconductor/solution interface. Fe^{3+} serves as a hole trap and Eu^{3+} as an electron trap in TiO_2 , respectively. The separation of the charge carrier is attributed to such trappings. In the meantime, Fe^{3+} and Eu^{3+} also speed up anodic and cathodic process via improving interfacial charge transfers. Superior photocatalysis of nanocrystalline TiO_2 co-doped with Fe^{3+} and Eu^{3+} ions was related to the cooperative actions of two dopants. (Note that at. % means atomic percentage)

Burns, et al., (2004) synthesized doped and undoped TiO_2 via sol-gel method under varying conditions to determine the effects of neodymium ion doping on the titania lattice. The doped titania nanoparticles were synthesized from titanium tetrachloride (TiCl_4), and neodymium(III) acetylacetonate hydrate. The reaction was performed at room temperature. The resulting yellow solution was allowed to rest until all gas evolution had ceased and the solution returned to room temperature. All samples were dip-coated onto quartz and boron-doped (p-type) silicon substrates. The coated substrates were allowed to dry in a desiccator, followed by calcination for 30 min in box furnace operating between 700 and 900 °C. Samples were characterized for their chemical composition by EDX and RBS and for their structure by XRD. The purpose of this study was to understand the effect of dopants, in particular neodymium, on the anatase to rutile transformation in TiO_2 . Both the transformation energy and the transformation temperature, measured from the annealing and XRD experiments, were found to increase with doping, with a maximum increase in activation energy occurring at 0.1 mol%. Higher concentrations of Nd^{3+} had no further effect on the phase transformation temperature or enthalpy. The anatase lattice was shown to deform predominantly along the c-axis to accommodate subsequently incorporated Nd^{3+} . The maximum in elongation of the c-axis also occurs at 0.1 mol%. This suggested some incorporation of Nd on the interstitial sites.

Zhang, et al., (2004) prepared Nd^{3+} , Pr^{3+} , Er^{3+} , and Dy^{3+} (0.25-5.0 at.%) doped nanocrystalline TiO_2 (Ln/TiO_2) by sol-gel process. A typical procedure is given below: these lanthanide oxide were dissolved in nitric acid and evaporated to dryness. The dry lanthanum nitrate was dissolved in butanediol and tetrabutyl-orthotitanate and added into solution at room temperature. A homogeneous transparent solution was formed and exposed in air for 1 week, a dry solid gel was obtained, which is further heated at 120°C for 5 h. The doped TiO_2 was finally obtained by heating the dry solid gel at different temperature for 1 h. Their activity of photodegradation of rhodamine B (RB) was investigated. Comparing with pure TiO_2 , these Ln doped TiO_2 exhibited much higher photoactivity. Both the concentration of lanthanide dopant and calcination temperature showed significant effect to the photodegradation of RB. The photocatalytic activity of pure TiO_2 was drastically decreased when calcination temperature was at 700°C , while the high photocatalytic activity was still maintained for Ln doped TiO_2 samples. HPLC-MS method was used to study the degradation process, and it demonstrated that the degradation of RB catalyzed by Ln doped TiO_2 principally went through a stepwise de-ethylation photochemical process.

Dopants are added to a wide variety of metal oxides in order to modify their properties. The goal in some case is to create or enhance desirable properties, while in others it is to eliminate or reduce undesirable effects. Dopant cations are classified as acceptor centers if their charge is less than that of the cation the replace, and donor centers if they have a greater charge. These labels recognize that the lattice defect that compensated an acceptor center can be replaced by holes under oxidizing conditions, while the lattice defect that compensates for the excess positive charge of a donor center can be replaced by electrons under reducing conditions (Smyth, et al., 2000).

The metal oxide such as titanium dioxide has recieved a lot of attension as a promising material for photocatalysis, liquid solar cell and degradation of pollutants. The photocatalytic efficiency of TiO_2 depends partially upon the relative degree of branching of the relative electron-hole pairs into interfacial charge-transfer reactions. In order to enhance interfacial charge-transfer reactions, the catalyst has been modified by selective metal ion doping of the crystalline TiO_2 matrix (Xu, et al., 2004).

The addition of a low percentage of metal was often proposed to improve the photocatalytic activity of TiO_2 . The metal may be introduced through different ways;

- Doping, i.e. molecular combination of metal oxide in the lattice of TiO₂. This process is expected to modify the band gap of the photocatalyst.

- Metallisation, i.e. deposition of noble metal on TiO₂ crystallites.

- Impregnation of TiO₂ with a salt of metal followed by evaporation, i.e. deposition of small amount of salt on TiO₂ surface.

- Addition of low concentration of transition metal to the solution of substrate to be treated (Rao, et al., 2003).

There are many applications involved the metal-doped TiO₂ in photocatalytic activity of many pollutants have shown as follows.

Allen, et al., (1992) synthesized rutile doped with Ni, Co, Fe, Pb, Cu, V and Mo ions by co-precipitation. The photoactivity of rutile TiO₂ may be reduced by doping it with certain transition metal ions. The dopant substitutes for the lattice titanium (IV) and this results in a greater annihilation of the higher energy photogenerated holes in the pigment by the 3d or 4d electrons of the dopants, which act as donors. Therefore on doping, the photoresponses of the pigments are enhanced the photoactivity of the pigment is decreased. Here, the recombination process is achieved by the impurity levels in the forbidden band of the TiO₂ polycrystal introduced by doping.

Brezova', et al., (1997) reported that the presence of metals, such as Li⁺, Zn²⁺, Cd²⁺, Pt⁰, Co³⁺, Ce³⁺, Cr³⁺, Mn²⁺, Al³⁺, and Fe³⁺, may significantly change the photoactivity of a TiO₂ layer prepared an glass fibre by the sol-gel method. The photoactivity is strongly dependent on the characterized and dopant concentration. The best results in term of phenol composition were obtained for dopant-free TiO₂, Li⁺/TiO₂, Zn²⁺/TiO₂ and Pt⁰/TiO₂ (Pt content, less than 5 mol/%Pt⁰: Ti⁴⁺) However, using Pt⁰/TiO₂ layers, they observed a slower decomposition of hydroquinone, which is produced as an intermediated by phenol hydroxylation. The presence of Co³⁺, Cr³⁺, Ce³⁺, Mn²⁺, Al³⁺ and Fe³⁺ ions in the TiO₂ photocatalyst (5 mol%Mn²⁺: Ti⁴⁺) has a detrimental effect on its photoactivity.

Wilke and Breuer (1999) investigated Cr³⁺ and Mo⁵⁺ doping on titania in order to study the different behaviour of n- and p-dopants. The adsorption of Rhodamine B (RB) on titania is

not influence by the incorporation of Cr^{3+} ions and no improvement over undoped titania is observed. At chromium concentrations below 1 at% both the lifetime and photocatalytic activity decrease drastically to remain nearly constant at a low level. This due to a low concentration Cr^{3+} ions can occupy regular lattice sites and act as traps. At higher Cr^{3+} concentrations interstitial sites are filled up obviously, due to the reduced lifetime fewer charge carriers can reach the surface and hence initiate degradation of the dye. For Mo^{5+} doped TiO_2 , at low Mo^{5+} concentrations the course of photodegradation and charge carrier lifetime is similar to that observed with Cr^{3+} doped TiO_2 samples. However, if the Mo^{5+} concentration is increased beyond 1 at% the influence of adsorption becomes predominant. Both adsorption and photodegradation increase. Since there is a higher surface coverage of the dye more charge carrier reaching the surface can contribute to the degradation process.

Murata, et al. (2000) investigated the effect of 4d and 5d transition elements on the photochemical properties of TiO_2 rutile. Rutile TiO_2 and $(\text{Ti},\text{M})\text{O}_2$ oxides (M: Nb,Mo,Ta, W) can be made by the oxidation of pure Ti and Ti - 5 mol% M alloys, respectively. The saturated photocurrent density of rutile $(\text{Ti},\text{M})\text{O}_2$ is dependent on the additional element, M, and it lowers in the order; Nb>Ta>Mo>W. The spectral dependence of anodic photocurrent density can be understood on the basis of the level structures calculated by the DV - X_∞ molecular orbital calculation.

Wang, et al. (2000) investigated lanthanide metal-ion-doped TiO_2 which prepared with hydrothermal method and characterized with XRD, TEM, ICP and fluorescence spectrum. The results showed that a small part of metal ions entered into the lattice of TiO_2 and others adsorbed on the surface of TiO_2 . The photocatalytic degradation of RB showed that the photoresponse of Eu^{3+} , La^{3+} , Nd^{3+} and Pr^{3+} doped TiO_2 electrodes were much larger than that of undoped TiO_2 electrode, indicating that the photogenerated carriers were separated more efficiently in Eu^{3+} , La^{3+} , Nd^{3+} and Pr^{3+} doped TiO_2 nanoparticles than in undoped TiO_2 nanoparticles.

Zhu, et al. (2000) synthesized Pt and Pd doped TiO_2 film on the silicon wafer using sol - gel method. After the films were reduced using H_2 in 400°C for 2 h, Pt existed as aggregated metallic Pt particles, while Pd existed as highly dispersed metallic Pd particles. The absorption

intensity for UV and visible light can be intensified significantly. This resulted from the interaction between highly dispersed Pd and the TiO₂ film. Pd atoms entered into the lattice of anatase TiO₂ film. The reduction of TiO₂ film doped with Pt cannot change the UV absorption due to the weak interaction between Pt and TiO₂ film.

Ranjit, et al., (2001) investigated the photocatalytic degradation of salicylic acid and *t*-cinnamic acid in aqueous suspensions of lanthanide oxide (Eu³⁺, Pr³⁺, Yb³⁺) doped TiO₂ photocatalysts. Complete mineralization has been achieved in the case of lanthanide oxide doped TiO₂ photocatalysts. The equilibrium dark adsorption of salicylic acid and *t*-cinnamic acid is ca three times and two times higher, respectively, on the lanthanide oxide modified TiO₂ photocatalysts as compared to the non-modified TiO₂ catalyst. The enhance degradation is attributed to the formation of the lewis acid-base complex between the lanthanide ion and the substrates at the photocatalyst surface.

Klosek and Raftery (2001) synthesized V-doped TiO₂ photocatalyst that is active under visible irradiation. The oxidation of ethanol over this catalyst was studied using ¹³C solid-state NMR methods that demonstrated that this catalyst photooxidized ethanol to produce mostly carbon dioxide with small amounts of acetaldehyde, formic acid, and carbon monoxide under visible irradiation. It is believed that under visible irradiation excited vanadium centers donate an electron to the TiO₂ conduction band, which allows the oxidation of surface adsorbed molecules. The activity of the TiO₂/V/PVG photocatalyst is greatly increased in comparison with the monolayer TiO₂/PVG photocatalyst under visible only irradiation.

Arana, et al., (2002) studied the photocatalytic degradation of maleic acid by using Fe-doped (0.15, 0.5, 2.0 and 5.0 % w/w in Fe) TiO₂. Catalysts with the lowest Fe content (0.15 and 0.5 %) showed a considerably better catalytic behavior than non-doped TiO₂ and catalytic with higher Fe contents.

Coronado, et al., (2002) reported that TiO₂, CeO₂/TiO₂ and CeO₂ materials were shown to present activity for toluene. In the case of the CeO₂/TiO₂ catalyst, EPR results indicated that photoactivation occurs on both components and had a limited charge transfer between both

components. The main effect of ceria incorporation to the titania sample is the partial blockage of the surface sites available for toluene photodegradation. The EPR study of the CeO₂ sample shows that UV illumination in the presence of oxygen induces the formation of O₂⁻ and the other radicals, which are derived from trapping of photogenerated electrons. The results of photocatalytic activity for toluene oxidation show that the photodegradation rate is slightly lower for CeO₂/TiO₂ than for the TiO₂ sample.

Abe, et al., (2003) investigated direct water splitting into H₂ and O₂ over Pt-loaded semiconductor photocatalysts. It was found that addition of a small amount of iodine anion, I⁻, into the aqueous suspension of Pt- TiO₂-anatase photocatalyst significantly improved the splitting into H₂ and O₂ with a stoichiometric ratio. The iodine anion was adsorbed preferentially onto Pt cocatalyst as iodine atom, I. This iodine layer effectively suppressed the backward reaction of water formation from H₂ and O₂ to H₂O over the Pt surface.

Rao, et al., (2003) studied the influence of metals: Ag⁺, Cu²⁺, and VO₃⁻ (vanadate) on the photocatalytic degradation of two typical azo dyes: AO-7 and tartrazine (Tart) and one nitroaromatic dye intermediate: 3-nitrobenzenesulfonic acid (3-NBSA). It was found that Ag⁺ has enhancing effect since it is easily reducible and act as electron traps. In contrast vanadate has a detrimental influence due to its anionic form. Cu²⁺ has no significant influence.

Tsuji, et al., (2003) reported that the modification of rutile TiO₂ by Ag negative-ion implantation found Ag nanoparticles formed in the surface layer of rutile. The photocatalytic efficiencies for Ag-implanted titania were evaluated by means of decolorization of methylene blue solution under fluorescent light. Ag-implanted rutile after annealing at 500 °C showed the better photocatalytic efficiency higher 2.2 times than that of unimplanted rutile titania. In the evaluation under fluorescent light through UV-cut filters, the Ag-implanted rutile showed 6.7 times better efficiency.

Sung-Suh, et al., (2004) examined the photocatalytic degradation of the rhodamine B (RB) dye in aqueous suspensions of TiO₂ and Ag-deposited TiO₂ nanoparticles under visible and UV light irradiation. The Ag deposits significantly enhanced the RB photodegradation under visible

light irradiation whereas the RB photodegradation under UV irradiation was slightly enhanced. The significant enhancement in the Ag-TiO₂ photoactivity under visible light irradiation can be ascribed to simultaneous effect of Ag deposits by both acting as electron traps and enhancing the RB adsorption on the Ag-TiO₂ surface.

Xie and Yuan (2004) prepared europium ion modified titania sol with anatase phase semicrystalline structure through coprecipitation and hydrochloric acid peptization route. Direct conversion of Eu³⁺-TiO₂ sol from amorphous to nanocrystalline phase was achieved at low temperature (70 °C) and high acidity (pH = 1.5). Eu³⁺-TiO₂ sol particles had narrow distribution with 7 nm in mean size and exhibited excellent interfacial adsorption capability to X-3B due to small size effect of sol particles and positive charge effect of europium ion. Electrons trapping process on sol particles resulted in lower photocurrent in Eu³⁺-TiO₂ sol system.

Liqiang, et al., (2004) prepared pure and La doped TiO₂ nanoparticles, and mainly investigated the relationships between PL spectra and photocatalytic activity. The results showed that La dopant had a great inhibition on TiO₂ phase transformation and did not give rise to a new PL signal, but it could improve the intensity of PL spectra with an appropriate La content, attributed to the increase in the content of surface oxygen vacancies and defects. In addition, the order of photocatalytic activity of La doped TiO₂ samples with different La content was the same as that of their PL intensity as following: 1 > 1.5 > 3 > 0.5 > 5 > 0 mol% La.

Wu and Chen (2004) synthesized vanadium doped TiO₂ catalysts by sol-gel method. The results show that the increase of vanadium doping promoted the particle growth, and enhanced red-shift in the UV-Vis absorption spectra. The photocatalytic activity was evaluated by the degradation of crystal violet (CV) and methylene blue (MB) under visible light irradiation. The degradation rate of CV and MB on V-doped TiO₂ were higher than those of pure TiO₂.

Besides metal doping on TiO₂ there have been also studies on phase change behavior of TiO₂ as follows.

Pekka Eskelinen (1993) investigated the anatase-rutile phase change temperatures in TiO_2 powders precipitated from aqueous TiCl_4 and the same deposited on muscovite and phlogopite micas. The anatase-rutile transformation of undoped TiO_2 took place between 750 and 800 °C. Doping with Al_2O_3 , NaCl , and SiO_2 increased the phase change temperature of supported and unsupported TiO_2 , but doping with $\text{FeCl}_3 \cdot 6\text{H}_2\text{O}$ decreased the beginning temperature of the phase change on unsupported TiO_2 . The difference in phase change dependence on temperature between undoped TiO_2 supported by micas and unsupported TiO_2 was caused by diffusion of aluminum, silicon, and sodium ions from the mica substrate during the calcination step. The crystal structure changes of the doped TiO_2 films supported by phlogopite behaved in the similar manner as those of the unsupported TiO_2 . Hence the small difference in the crystal structure of muscovite and phlogopite did not have any effect on the crystal structure of TiO_2 supported by either micas.

Bregani, et al., (1996) investigated the substitution effect of TiO_2 by Mo and W ions on the stability of anatase studied by XRD, TEM, and surface area measurements in the 300-1000 K temperature range. The powder containing W shows smaller microstrains compared to those of pure anatase phase, while larger microstrains are found for the Mo- TiO_2 powder. The anatase to rutile transformation caused by annealing is proposed to be related to the disappearance of Ti^{3+} ion in the anatase structure. Finally, a possible redox mechanism $\text{Ti}^{3+} \leftrightarrow \text{Ti}^{4+} + e^-$ is proposed to play a fundamental role in the catalytic and sensor properties of these material.

Zhang and Reller (2001) prepared nanocrystalline mesoporous iron -doped TiO_2 by sol-gel method. It was found that the as-prepared solids exhibit a narrow size distribution and that the iron is homogeneously distributed in the TiO_2 matrix. The influence of the iron concentration on the phase transformations of the doped TiO_2 was investigated by X-ray diffractometry. The transition of pure TiO_2 from the amorphous state to anatase is observed at a lower temperature than for iron doped titania. For pure TiO_2 transformation from anatase to rutile takes place at 500 °C, i.e. at much lower temperatures than that of iron-doped TiO_2 (transition temperature : 600 °C). It showed that the remarkable shift of crystallization and of the phase transition from anatase to rutile to higher temperatures is caused by structural iron doping, i.e. the substitution of titanium ions by iron ions within the structural framework. The formation or segregation of the iron content and the calcination temperature. XRD and TEM results indicate that

the iron doping decreases the grain growth rate, i.e. sintering process, and therefore leads to higher surface areas. The formation of the iron titanium oxide pseudo brookite, $\text{Fe}_2\text{Ti}_2\text{O}_5$, was observed above 670°C , but only for an iron content of more than 3 atom%.

Zhang and Reller (2002) investigated the influence of altrivalent cation doping of TiO_2 on its phase transition and grain growth. It is shown that dopants like Fe^{3+} , Si^{4+} , V^{5+} , Ru^{3+} , and Ni^{2+} affect the phase transition temperature of the titania host, and that significant variation is observed for silicon doping. Compared to the iron- and silicon-doped system, which show a significant grain growth hampering trend, the vanadium, nickel, and ruthenium dopants exhibit very small effects on the retardation of the grain growth. This indicates that different cations have different effects on the grain growth mechanism of the TiO_2 host during heat treatment process. However, these dopants still influence the phase transformation temperature of the titania. All of the ruthenium, nickel and vanadium dopants catalyze the transition of anatase to rutile, and this phenomenon is especially manifested at high dopant concentrations. The formation of anatase from amorphous phase needs higher temperature for either nickel- or vanadium-doped samples than that of pure titania. Oppositely, the amorphous-to-anatase transformation is observed at lower temperatures for ruthenium-doped samples. The sequence of arresting grain growth is following: $\text{Si}^{4+} > \text{Fe}^{3+} > \text{V}^{5+} > \text{Ru}^{3+} > \text{Ni}^{2+}$.

Saila Karvinen (2003) investigated the effect of trace element doping of TiO_2 on the crystal growth and on the anatase-to-rutile phase transformation of TiO_2 . The co-precipitation process, from sulfate solution, of doped (Cr, Fe, V, Nb, Si, P) TiO_2 was also studied. The heating temperature were 473, 673, 873, 993, 1133 K and higher temperature needed to achieve a rutile content of 98-99%. Anatase-to-rutile transformation was accelerated by the mmol% content of Nb, Cr, Si, and Fe in TiO_2 . Interaction of co-precipitated or impregnated cations was found critical in the phase transformation process. Nb retarded the crystal growth during calcination. Sulfate ions minimized the specific surface area of TiO_2 serve to promote the development of new high-technology TiO_2 products for photocatalytic purposes.

Ruiz, et al., (2004) reported that La-doped TiO_2 and Cu/La-doped TiO_2 powders were characterized by XRD in order to study the influence of these additives on the growth

inhibition and phase transformation of nanosized TiO_2 . The results show that La retarded the transition phase to higher temperatures and hindered the grain growth of titania. Both samples loaded with 5 and 10 at% of La presented pure anatase phase at 700 °C, whereas bare TiO_2 has already undergone a transformation to rutile, and were predominantly anatase at 800 °C. The grain growth for these samples was strongly suppressed. According to XRD analyses, at 800 °C, the grain size was about 11 nm for 5 at% of La and only 7 nm in the case of 10 at% La doping. If we add 2 at% of Cu was added to the La-doped samples, pure anatase was still found at 700 °C. However, the phase transformation was no longer inhibited and the form observed at 800 °C was primarily rutile. A ternary La-Ti phase ascribed to $\text{La}_4\text{Ti}_9\text{O}_{24}$ was segregated in all the doped samples when the transformation to rutile occurred.

Recently, there has been increasing interest in application of nanocrystalline materials for catalyst, supports, ceramics, inorganic membranes, gas sensing, water purification, and solar energy conversion (Yanging, et al., 2001). Furthermore, photocatalysis of nanocrystalline titanium dioxide has a great many advantage on waste water treatment such as high catalysis efficiency, energy saving, no pollution, etc. and can degrade all kinds of organic pollutants from water effectively. All of those merits make photocatalysis of water treatment and it is supposed to be used widely in the future (Baolong, et al., 2003).

Coloration is a key factor in the commercial success of textile products, particularly those with a high fashion content, especially garments, furnishings and upholstery. The business generated by the dye industry over the last two years was approximately US\$ 22 billion, and constituted a total employment of about 1.45 million people. Excluding fluorescent brighteners, the dye consumption per capita is approximately 150 g per year, serving an average consumption of textile fiber of about 14.0 kg per year per inhabitant. Despite, the high economic importance of the textile industry in the world, this industry is responsible for around 700,000 t of about 10,000 different types of dyes on pigments produced each year. During dye use among the several industries responsible for pollution of the aquatic ecosystems, the textile dyeing and printing industries are major players, around a half of a tonne of these dyestuffs are lost per day to the environment. Approximately 200 l of water are required, for every kilogram of finished cotton fabric. The reactions necessary to fix these dyes to the fibers are not very efficient. Therefore, residual dyes, several types of chemicals and salts are dumped into the water and are discharged in

the wastewater system. At least 20% of those not used dye might enter the environment through effluents from wastewater treatment plants (Carneiro, et al., 2004).

Removal of color in wastewater generated by the textile industries is color issue of discussion and regulation all over the world. Among the relative dyes, the textile azo dyes with synthetic intermediates as contaminant and its degradation products, have undoubtedly attracted the most attention with regard to high environmental impact, because of their widespread use, their potentiality to form toxic aromatic products (carcinogenicity and mutagenicity properties) and their low removal rate during primary and secondary treatment. They represent about 50% of the worldwide production and correspond to an important source of contamination considering that a significant part of the synthetic textile dyes are lost in waste streams during manufacturing or processing operations. Therefore it is important to develop effective wastewater remediation technologies for these compounds.

Various chemical and physical treatment processes are currently proposed for these dyes. These largely fall into the categories of direct precipitation or elimination by adsorption, flocculation, membrane separation, coagulation and chlorination. These methods have been largely incomplete and ineffective because the problem is not completely resolved, being required further treatment. A number of biological processes, such as sequenced anaerobic / aerobic digestion, have been proposed in the treatment of textile wastewater, but they are limited due to the fact that many of the dyes are xenobiotic and non-biodegradable. Alternative methods based on advanced oxidation processes combining ultraviolet irradiation and oxidative agents for dye treatment have been also investigated, but the presence of intermediates arising from the photodegradation reaction could be more harmful than the pollutant itself.

The attractiveness of the heterogeneous photocatalytic oxidation processes in providing a definite solution for the conversion of textile organic compounds lies in the fact that they can be used as a tertiary treatment process and the resulting water can be recycled or re-used in a competitive way. Among several photocatalyst (TiO_2 , WO_3 , SnO_2 , ZnO , CdS and others) acting via hydroxyl radical generation as powerful oxidant, the TiO_2 semiconductor under UV irradiation has been the preferred catalyst largely due to its photo-stability, non-toxicity, low cost and water insolubility under most environmental condition (Carneiro, et al., 2004).

The efficiency of advanced oxidation processes for degradation of recalcitrant compounds has been extensively documented. Photochemical processes are used to degrade toxic

organic compounds to CO_2 and H_2O without the use of additional chemical oxidants, because the degradation is assisted by high concentrations of hydroxyl radicals generated in the process. In this case, the photoexcitation of TiO_2 particles promotes an electron from the valence band to the conduction band, generating an electron/hole pair. Both reductive and oxidative processes can occur at or near the surface of the photoexcited TiO_2 particle. In general, oxygen is used to scavenge the conduction band electron, producing a superoxide anion radical, effectively preventing electron/hole recombination, and prolonging the lifetime of the hole. The photogenerated hole has the potential to oxidize several substrates by electron transfer. In aqueous solutions, oxidation of water to hydroxyl radical by the photogenerated hole appears to be the predominant pathway. Hydroxyl radicals and, to a lesser extent, superoxide anion can act as oxidants, ultimately leading to the mineralization of organic compounds (Gome de Moraes, et al., 2000).

The mineralization of most of the organic pollutants could be degrade following the usually proposed mechanism; which the heterogeneous photocatalytic oxidation processes shown in Figure 5.

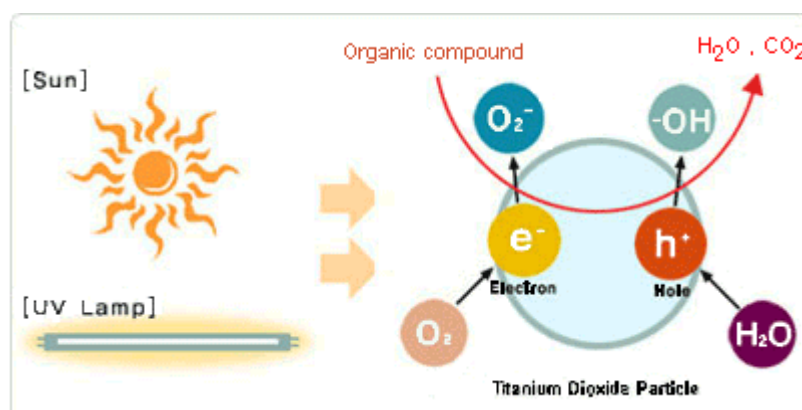


Figure 5 The heterogeneous photocatalytic oxidation processes of titanium dioxide photocatalyst. (www.inno.com.hk/Products/)

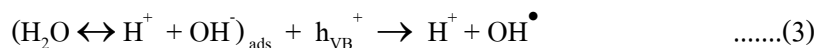
1. Absorption of efficient photons ($h\nu > E_g = 3.2 \text{ eV}$) by titania



2. Oxygen ionosorption (first step of oxygen reduction; oxygen's oxidation degree passes from 0 to -1/2)



3. Neutralization of OH^- groups by photoholes which produces OH^\bullet radicals



4. Neutralization of $\text{O}_2^{\bullet-}$ by protons



5. Transient hydrogen peroxide formation and dismutation of oxygen



6. Decomposition of H_2O_2 and second reduction of oxygen



7. Oxidation of the organic reactant via successive attacks by OH^\bullet radicals



8. Direct oxidation by reaction with holes



As an example of the last process, holes can react directly with carboxylic acid generating CO_2



In most cases, the degradation is conducted for dissolved compounds in water with UV-illuminated titania. The possible extents of the technique concern the irradiation source and the physical state of the pollutant. Recently, some works have reported the degradation of organic dyes induced by visible light by photosensitization. The interest is to use solar visible light which is free and inexhaustible (Houas, et al., 2001).

In the present work, it was attempted to establish the degradation of a dye present in colored aqueous effluents from textile industries. The model dye chosen was methylene blue (MB).

Methylene blue, MB, is a brightly coloured, blue cationic thiazine dye, with λ_{max} values at 660, 614 and 292 nm. The uses of MB include being an antidote for cyanide poisoning in humans, antiseptic in veterinary medicine and, most commonly, in vitro diagnostic in biology, cytology, hematology and histology. The structure of methylene blue shows in Figure 6.

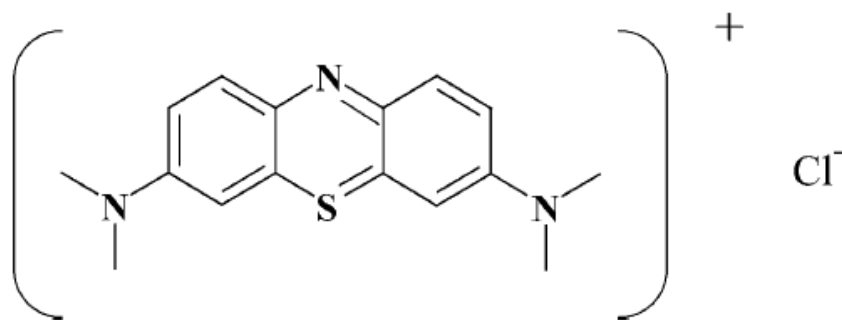


Figure 6 The structure of methylene blue (Mills et al., 1999).

The doubly reduced form of MB, leuco-methylene blue, i.e., LMB, is colourless (typically, $\lambda_{\max} = 256 \text{ nm}$) and stable in de-aerated aqueous solutions. The singly reduced form of MB, the semi-reduced radical, $\text{MB}^{\bullet-}$, is pale yellow ($\lambda_{\max} = 420 \text{ nm}$) and readily disproportionates ($k = 3 \times 10^9 \text{ dm}^3 \text{ mol}^{-1} \text{ s}^{-1}$) to form MB and LMB, i.e.,

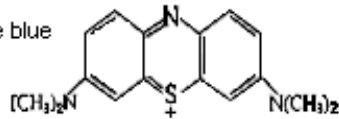
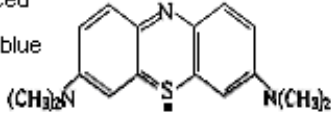
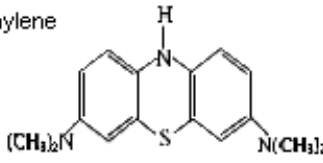
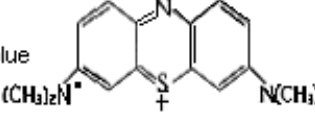


Less research has been conducted into the oxidised form of MB, i.e., $\text{MB}^{\bullet+}$, $\lambda_{\max} = 520 \text{ nm}$, which appears to be quite stable and it easily reduced back to MB in acidic solution, but decomposes irreversibly in slightly alkaline ($\text{pH} = 9.1$) solution. MB readily forms dimers in aqueous solution, i.e.,



A typical value for K_D , the equilibrium constant associated with the dimerisation process, is $3970 \text{ dm}^3 \text{ mol}^{-1}$. The structures of most of the methylene blue-type compounds highlighted above are illustrated in Table 4 along with the associated pKa and redox potential data.

Table 4 Structure and UV-Vis absorption characteristics of methylene blue and its common

Species	Structure	Abbreviation	pK _a	E ⁰ vs. NHE (V)	λ _{max}	Other properties
Methylene blue		MB	0		660, 614, 292	K _D = 3970 dm ³ mol ⁻¹
Semi-reduced methylene blue		MB ^{•-}	-3,2,9	(MB/MB ^{•-}) = -0.23	420	Readily disproportionates to form MB and LMB
Leuco methylene blue		LMB	4,5,5,8	(MB/LMB) = 0.011 (pH 7) and 0.532 (pH 0)	562	
Oxidised methylene blue		MB ^{•+}		(MB ^{•+} /MB) = 1.08	52012	Stable in acid (pH 1) and unstable at pH 9

The photochemistry of MB has been widely studied. MB remains a popular dye sensitiser in photochemistry especially in the areas of singlet oxygen production and reductive electron transfer. The wide and varied use of MB in photochemistry is attributable to its relatively long-lived, triplet state, $\tau_T = 450 \mu\text{s}$, with its high probability of formation, $\phi_T = 0.52$, large energy (1.44 eV above the ground state) and high triplet oxidation potential $E^0(\text{MBT} / \text{MB}^{\bullet+}) = 1.21 \text{ V}$ versus NHE. The major photophysical and redox characteristics of MB are summarised in Table 5 (Mills et al., 1999).

Table 5 Photophysical properties of methylene blue (Mills et al., 1999).

	Singlet: MB ¹	Triplet: MB ³
ϕ_T	-	0.52
E (excited state) (kJ mol ⁻¹)	180	138
τ	30-390 ps	450 μ s
ϕ (fluorescence)	0.04	-
E ⁰ (excited state/ MB [•]) vs. NHE (V)	1.60	1.21

Given the well-established photochemical activity of MB, initially it might appear surprising to note that MB has often been used as a reactant in semiconductor photocatalysis. This surprise may well increase when it is realised that the semiconductor most often employed in such studies is TiO₂, a UV absorber. However, a brief inspection of the UV-Vis absorption spectra of MB, illustrated in Figure 7 (solid line), reveal that MB adsorbs a little light between 300 and 400 nm. The latter wavelength region is usually the region of illumination in TiO₂-sensitised semiconductor photocatalysis, since most UV irradiation sources used in such work are designed to emit light of $\lambda < 400$ nm, and most of the glassware used is Pyrex, which cuts off at 300-310 nm. To emphasise the latter point a little further, the relative emission intensity versus λ profile for one of the most common light sources in use in semiconductor photocatalysis, the blacklight bulb (λ_{\max} (emission) = 355 nm), is also illustrated in Figure 7 (dotted line). A brief inspection of the two spectra in Figure 7 reveals a marked lack of overlap. As a result, it is not surprising that most workers find that aqueous solutions of MB show in the absence of TiO₂ and in the absence or presence of oxygen (Mills et al., 1999).

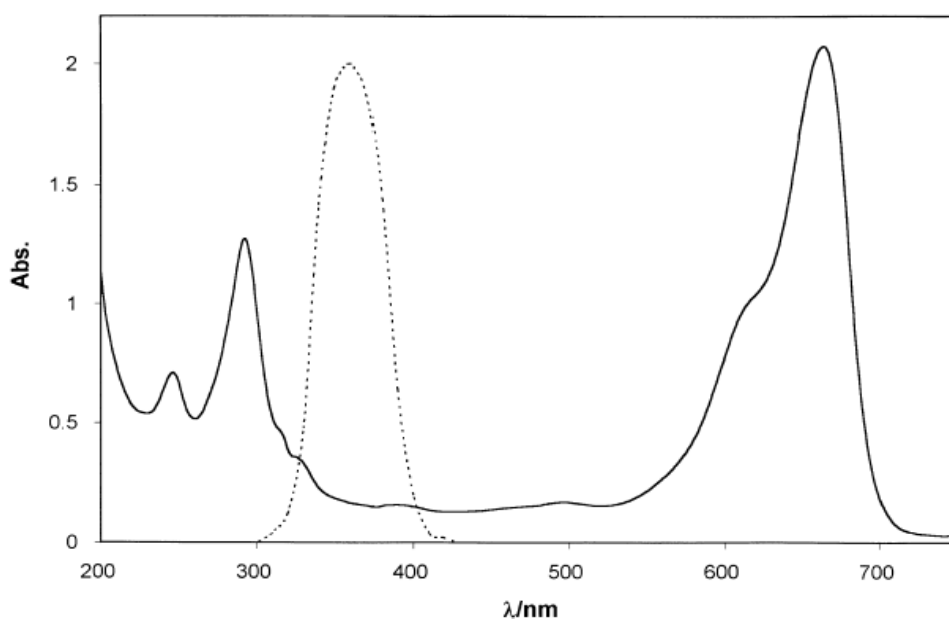


Figure 7 UV-Vis absorption spectrum of MB aqueous solution (solid line) and the relative emitted light intensity (dotted line) for 8W blacklight bulb (Mills et al., 1999).

Many studies for photochemistry of MB, others textile dyes and pollutants are as follows.

Herrmann, et al., (1997) synthesized TiO_2 and Ag-TiO_2 catalysts supported thin layer by a dip-coating procedure on quartz substrate. The resulting materials have been characterized by SEM/EDX, XRD, XPS and UV-Vis absorption spectroscopy. The immobilized catalysts were tested in the photocatalytic degradation of malic acid. For this reaction, the presence of metallic silver does not produce an intrinsic increase in photocatalytic activity in comparison with pure titania. The apparent increase observed in activity is principally due to the increase in the exposed surface due to the textural characteristics of the Ag-TiO_2 layer in comparison with TiO_2 . In addition, a previous treatment of the deposited Ag-TiO_2 samples under UV light just after calcination induces a slightly higher photocatalytic activity, whatever the expression chosen for it. This has to be ascribed to a partial photoreduction of Ag^+ ions into Ag^0 atoms which can agglomerate, as small metallic clusters identical to those found in photographic process. Metallic silver in low amounts can play a favourable role by attracting electrons, thus helping the electron-

hole pair separation and preventing the electron-hole recombination. The improvement in quartz-deposited titania by addition of Ag^+ ions and UV pretreatment is about 12%. A careful comparison of the photocatalytic activity of supported titania samples with bulk TiO_2 Degussa P-25 shows a decrease in activity. This effect should be compensated by the benefit of avoiding filtration of small particles.

Ohno, et al., (1999) prepared Ru-doped TiO_2 particles and investigated their properties as the photocatalyst under visible light. With this photocatalyst, the oxygen evolution reaction occurred by irradiation of visible light at wavelengths longer than 440 nm using iron(III) ions as the electron acceptor. To clarify the mechanistic aspects of the effect of Ru-doping, photoelectrochemical properties of Ru-doped TiO_2 sinter electrode were investigated. The activity of the Ru-doped TiO_2 powder for the photo-oxidation of water was dependent on the doping concentration, and was highest at about 0.007 wt.% Ru. The quantum efficiency of the reaction was 0.14% at 435 nm, which was observed using the powder doped with 0.007 wt.% Ru and calcined at 1200°C . Although the efficiency is still low, it is important that the oxidation of water is demonstrated under visible light using the Ru-doped TiO_2 powder. For the photocatalysts doped with a large amount of Ru, the activity is lowered probably by the formation of recombination centers at high concentrations. To prevent the generation of the recombination centers, the ion-implantation method may be useful.

Xu, et al., (1999) synthesized ultrafine TiO_2 particles by sol-gel method and studied the influence of particle size of TiO_2 on the photocatalytic degradation of methylene blue (MB) in aqueous solution. The results suggested that the adsorption rate and adsorbability of MB on suspended TiO_2 particles increased as the particle sizes of TiO_2 decreased. Photocatalytic activity of TiO_2 also increased as the particle sizes of TiO_2 became smaller, especially when the particle size is less than 30 nm. The half-life of the photocatalytic degradation of MB also decreased as the particle sizes of TiO_2 decreased. The first order reaction rate constant for photocatalytic degradation of MB increased as particle size of TiO_2 decreased. The initial degradation rate of MB in a suspended model was higher than that of a fixed-bed model. This will overcome the difficulty of preparation of ultrafine TiO_2 particles. The industrialization of the TiO_2 suspended-type photoreactor will be

easier once the problem of separation of fine TiO₂ particles is solved. The application of the ceramic membrane for this problem is now in progress and will be published.

Ding, et al., (2000) prepared a series of TiO₂ samples with different anatase-to-rutile ratios, and studied the roles of the two crystallite phase of TiO₂ on the photocatalytic activity in oxidation of phenol in aqueous solution. High dispersion of nanometer-size anatase in the silica matrix and the possible bonding of Si-O-Ti in SiO₂/TiO₂ interface were found to stabilize the crystallite transformation from anatase to rutile. The temperature for this transformation was 1200^oC for the SiO₂/TiO₂ sample, much higher than 700^oC for Degussa P25 TiO₂. It is shown that samples with higher anatase-to-rutile ratios have higher activities for phenol degradation. However, the activity did not totally disappear after a complete crystallite transformation for P25 TiO₂ samples, indicating some activity of the rutile phase. Furthermore, the activity for the SiO₂/TiO₂ samples after calcination decreased significantly even though the amount of anatase did not change much. The activity of the same samples with different anatase-to-rutile ratios is more related to the amount of the surface-adsorbed water and hydroxyl groups and surface area, leading to the decrease in activity.

Houas, et al., (2001) investigated the TiO₂/UV photocatalytic degradation of MB in aqueous solution. In addition to a prompt removal of the color, TiO₂/UV-based photocatalysis was simultaneously able to oxidize the dye, with an almost complete mineralization of carbon and of nitrogen and sulfur heteroatoms into CO₂, NH₄⁺, NO₃⁻ and SO₄²⁻, respectively. A detailed degradation pathway has been determined by a careful identification of intermediate products, shown in Figure 8, in particular aromatics, whose successive hydroxylation lead to the aromatic ring opening. It can be concluded that photocatalysis can decontaminate colored used waters. Photocatalysis appears as the only sub-discipline of heterogeneous catalysis, which is able to convert organic pollutants to CO₂ in water without heating nor using high pressure of oxygen nor requiring chemical reactants or additives. These results suggest that TiO₂/UV photocatalysis may be envisaged as a method for treatment of diluted wastewater in textile industries.

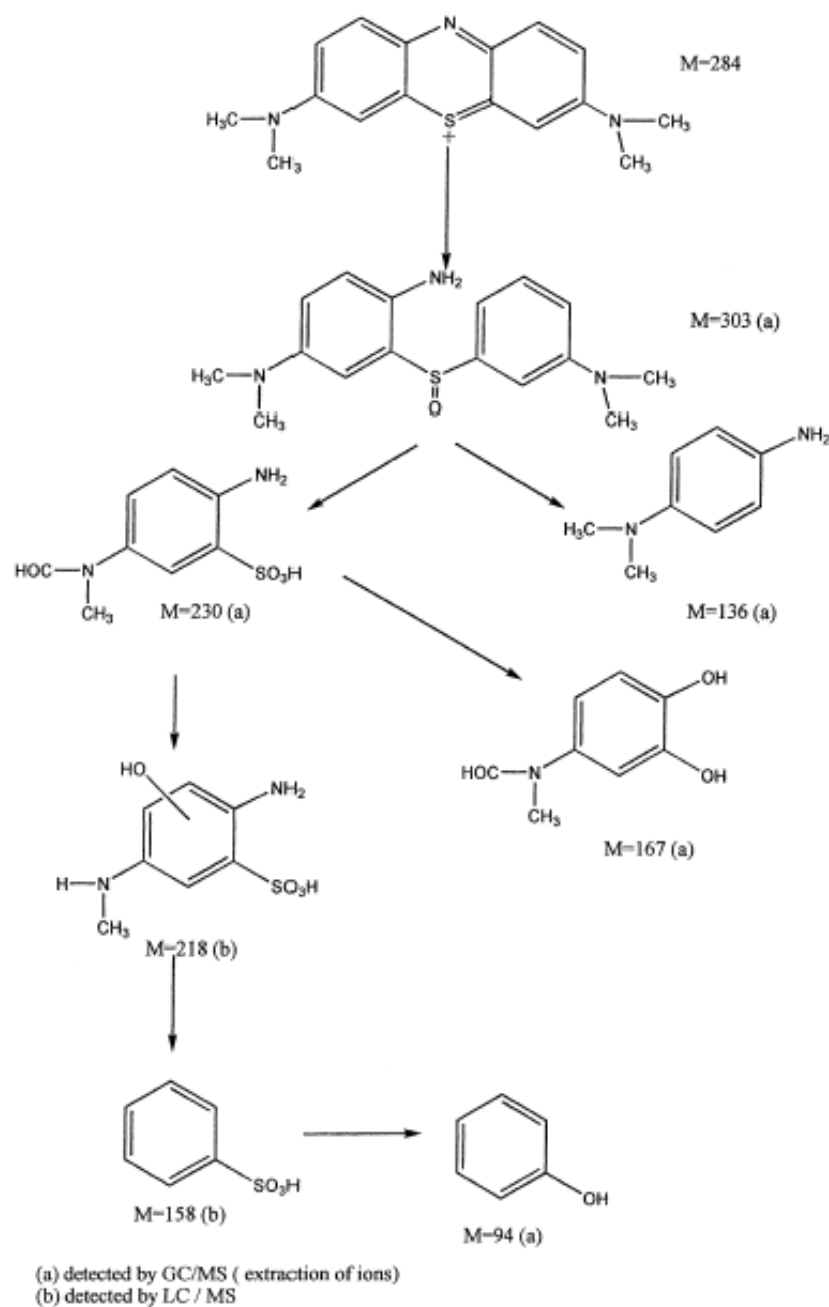


Figure 8 Photocatalytic degradation pathway of methylene blue (Houas, et al., 2001).

Yamashita, et al., (2002) investigated the metal ion-implantation of TiO_2 with metal ions (V^+ , Mn^+ , Fe^+) at high energy acceleration. The UV-Vis absorption spectra of these metal ion-implantation of TiO_2 were found to shift toward visible light region depending on the amount and the kind of metal ion-implanted. These catalysts exhibited photocatalytic reactivity for degradation of 2-propanol diluted in water under visible light irradiation. The investigation using

XAFS analysis suggested that the implanted metal ions are located at the lattice positions of Ti^{4+} in TiO_2 after the calcination. These spectroscopic studies show that the substitution of Ti ions in TiO_2 lattice with implanted metal ions is important to modify TiO_2 to be able to adsorb visible light irradiation. The results of the ab initio molecular orbital calculation indicated that in the metal ion-implanted TiO_2 the overlap of the conduction band due to Ti(d) of TiO_2 and the metal(d) orbital of the implanted metal ions can decrease the band gap of TiO_2 to enable to absorb the visible light. From photocatalytic reactivity for degradation of 2-propanol found that the excess amount of implanted metal ions probably brings about the increase of deposited metal ions which cover the top surface of catalyst and suppress the photocatalytic reaction. These results indicate that the moderate amount of implanted metal ions is suitable to realize the efficient photocatalytic reaction under visible irradiation.

Di Paola, et al.,(2002) prepared polycrystalline TiO_2 photocatalyst loaded with various ions of transition metals (Cr, Co, Cu, Fe, Mo, V, and W) by using the wet impregnation method. The samples were characterized by using some bulk and surface techniques. The samples were employed as catalysts for 4-nitrophenol photodegradation in aqueous suspension. The characterization results have confirmed the difficulty to find a straightforward correlation between photoactivity and single specific properties of the powders. The impregnated samples revealed recombination rate always higher than that of bare TiO_2 . The photoactivity of TiO_2 was reduced by the presence of transition metal ions with the exception of W, which instead played a beneficial role. This effect was more significant as the amount of loaded metal increased. The results of femtosecond pump-probe diffused reflectance spectroscopy appear quite in accord with the observed photocatalytic activity only for the lowest values of electron-hole recombination rate of the samples. The photoactivity of the powders roughly decreases according to the following sequence: $\text{TiO}_2/\text{W} > \text{TiO}_2/\text{Mo} > \text{TiO}_2/\text{Cu} > \text{TiO}_2/\text{Fe} \sim \text{TiO}_2/\text{Co} > \text{TiO}_2/\text{V} > \text{TiO}_2/\text{Cr}$.

Chiang, et al., (2002) synthesized copper(II) oxide loaded onto the surface of Degussa P25 TiO_2 particles by photodecomposition. The doped sample was subsequently utilized as the photocatalyst for cyanide oxidation. The copper content on the TiO_2 surface was varied from 0.05 to 10.0 at.% of Cu. It was found that nanosized CuO deposited were present on the surface of TiO_2 . Modifying TiO_2 with CuO changed the optical properties of TiO_2 and the onset of absorption

was red shifted. The photocatalytic activity of the CuO loaded TiO₂ was measured to determine their ability to oxidize cyanide. It was found that the rate of photooxidation of cyanide assisted with the doped catalyst was improved slightly at 0.10 at.% Cu. Any further increase of the copper dopant concentration decreased the oxidation rate remarkably. The decrease in the activity was explained in terms of the competition reaction of Cu(II) cyanide complex ions for surface hydroxyl radical. In all cases cyanide was being oxidized to cyanate, the end product of cyanide photooxidation.

Stylidi, et al., (2003) investigated the photocatalytic degradation of Acid Orange 7 (AO-7) in aqueous TiO₂ suspensions with the use of a solar light simulating source. The photoreaction was followed by monitoring the degradation of the dye and the formation of intermediates and final products, as a function of time of irradiation, both in solution and on the photocatalyst surface. It has been found that the process leads to decolorization and, eventually, to complete mineralization of the dye solution. Evolution of intermediates and final products on both the photocatalyst surface and the solution has been monitored with a variety of techniques, which enable the identification of the reaction pathway, from adsorption of the dye molecule on the photocatalyst surface, to the formation of final products. AO-7 adsorbs on the photocatalyst surface via the oxygen of its hydrazone form and the two oxygen atoms of the sulfonate group. The tautomeric forms of AO-7 in solution shown in Figure 9. Interaction with solar light results, initially, in cleavage of the dye molecule in the vicinity of the azo bond and the formation of molecules containing naphthalene- and benzene- type rings. This step, which takes place, to a significant extent, via the photosensitized mechanism, results in decolorization of the solution but is not accompanied by significant decrease of the COD.

The primary reaction intermediates undergo a series of successive oxidation steps which lead to the formation of aromatic acids and then to aliphatic acid of progressively lower molecular weight. This results in the decrease of pH and an increase of the conductivity of the solution. Eventually, complete mineralization of carbon and of nitrogen and sulfur heteroatoms is achieved, into CO₂, NH₄⁺, NO₃⁻ and SO₄²⁻, respectively. A TiO₂-mediated photodegradation mechanism for AO-7 is proposed on the basis of quantitative and qualitative detection of intermediate compounds that shown in Figure 10.

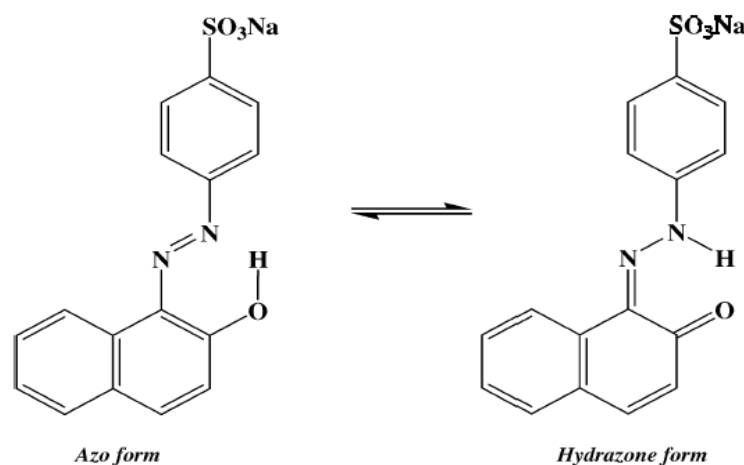


Figure 9 Tautomeric forms of Acid Orange 7 in solution (Stylidi, et al., 2003).

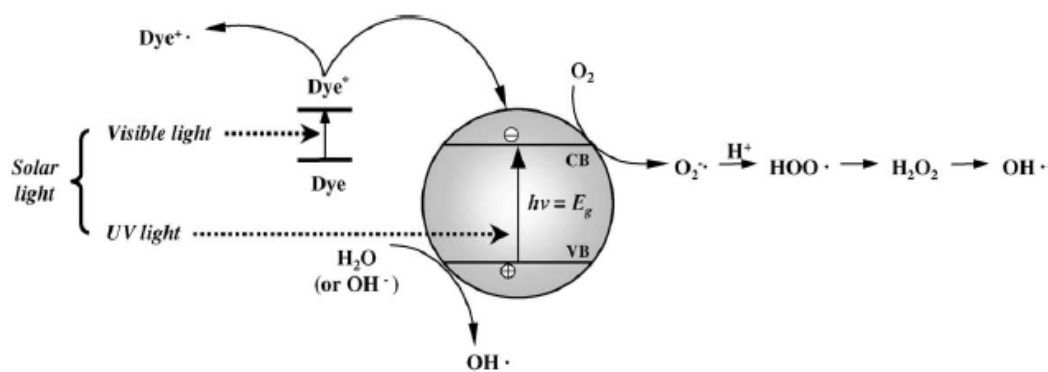


Figure 10 Schematic presentation of the mechanisms of generation of oxidative species, following excitation of the AO-7/ TiO₂ system with solar light (Stylidi, et al., 2003).

Arabarzis, et al., (2003) investigated nanocrystalline titania thin film photocatalysts by gold deposition via electron beam evaporation, with an attempt to study decomposition reaction rate of industrial water pollutants. The materials were characterized and their photocatalytic activity was tested for methyl orange photodegradation. The surface deposition of gold particles improves the photocatalytic efficiency of the titania films by the synergetic action on the charge separation process onto the semiconductor. The most advantageous surface concentration of gold particles in the composite Au/TiO₂ photocatalyst was found to be 0.8 μg cm⁻², leading to a two times faster degradation of methyl orange with respect to the rate obtained with the original TiO₂ material. Higher surface loading result in an efficiency decrease, and this can be understood in terms of an optimum gold particle size and surface characteristics as well as the semiconductor availability for

light absorption and pollutant adsorption. The improvement in the photocatalytic efficiency of titania films by gold ions deposition is more than 100%. This enhancement is attributed to the action of Au particles, which play a key role by attracting conduction band photoelectrons and preventing electron-hole recombination.

Matsuo, et al., (2004) examined the defect of simply adsorbed Sm, Eu, and Yb ions on TiO_2 (Ln/TiO_2) and Fe ions adsorbed onto TiO_2 (Fe/TiO_2) from the photocatalytic decomposition of adenosine 5'-triphosphate (ATP) as an anionic substance, 2-propanol as a neutral substance, and methylene blue (MB) as a cationic substance. The amount of ATP disappearing in 40 min of reaction in the presence of Ln/TiO_2 increase in the order: $\text{Ln}-\text{Sm} < \text{Eu} < \text{Yb}$. For 2-propanol, the photocatalytic activity of Ln/TiO_2 catalyst were similar to that of unmodified TiO_2 (u-TiO_2) catalyst. For MB, the photocatalytic activities of Ln/TiO_2 catalyst were less than that of u-TiO_2 catalyst. By contrast, Fe/TiO_2 catalyst was excellent in photocatalytic decomposition of ATP, 2-propanol and MB. The photocatalytic activity of $\text{Yb}/\text{TiO}_2\text{-C}$ calcined at 500°C for 1 h decreased for ATP, slightly decreased for 2-propanol, and increased for MB compared with Yb/TiO_2 . Photocatalytic activities of $\text{Fe}/\text{TiO}_2\text{-C}$ for ATP, 2-propanol and MB were all less than that of Fe/TiO_2 . Since EXAFS revealed that the coordination structure around Yb(III) ions on the surface of TiO_2 in Yb/TiO_2 was like a hydrated structure including chloride ions, and that in $\text{Yb}/\text{TiO}_2\text{-C}$ was like an oxide structure, the difference in photodegradation between Fe/TiO_2 and $\text{Fe}/\text{TiO}_2\text{-C}$ is believed to be a result of the coordination structure around Fe(III) ions on the surface of TiO_2 . These facts together suggest that the selectivity of photocatalytic decomposition for target substances can be controlled and is a combination of the properties of adsorbed metal ions (e.g. ionic radius, d-electron or f-electron, redox potential) and the coordination structure of their ions on the surface of TiO_2 . In the present study, Sm/TiO_2 , Eu/TiO_2 , and Yb/TiO_2 are more selective toward anionic substances than Fe/TiO_2 , which is excellent for decomposition of ionic and neutral substances.

Xie and Yuan (2003) prepared the cerium ion (Ce^{4+}) modified titania sol and nanocrystallites by chemical coprecipitation-peptization and hydrothermal synthesis methods, respectively. XRD patterns show that $\text{Ce}^{4+}\text{-TiO}_2$ sol particles had anatase semicrystalline structure. And the calcined $\text{Ce}^{4+}\text{-TiO}_2$ powder was composed of predominant anatase titania and crystalline cerium titanate (11.18 wt.% $\text{Ce}_x\text{Ti}_{(1-x)}\text{O}_2$). AFM micrograph shows that ultrafine particles were well

dispersed in sol system and average particle size was about 10 nm. Ce^{4+} - TiO_2 crystallites have grown into 70 nm in mean size. The difference in calculated particle size (2.41 nm for sol particle and 4.53 nm for crystallite) by XRD Scherrer's formula was mainly due to aggregation effect of nanoparticles. The experimental results showed that Ce^{4+} - TiO_2 sol and nanocrystallites can effectively photodegrade reactive brilliant red dye (X-3B) with the dye/ Ce^{4+} - TiO_2 /visible light reaction system. Moreover, photocatalytic reaction also can carry out in hydrosol system as well as in suspension reaction system. The overall photocatalytic degradation efficiency was observed to decrease in order : Ce^{4+} - TiO_2 sol > Ce^{4+} - TiO_2 crystallites > P25 TiO_2 . The difference of photoactivity in photodegradation reaction was ascribed to the particle size, morphology, and electrons scavenging effect. And photocatalytic reaction mechanisms involving photolysis, photocatalysis, photosensitized photocatalysis and interband photocatalysis were proposed regarding different photocatalytic reaction system that shown in Figure 11-14. It was experimentally verified that photocatalytic reaction in the sol system was feasible. The capability of dye photodegradation by sol particles under visible light is a very exciting aspect in photocatalytic area.

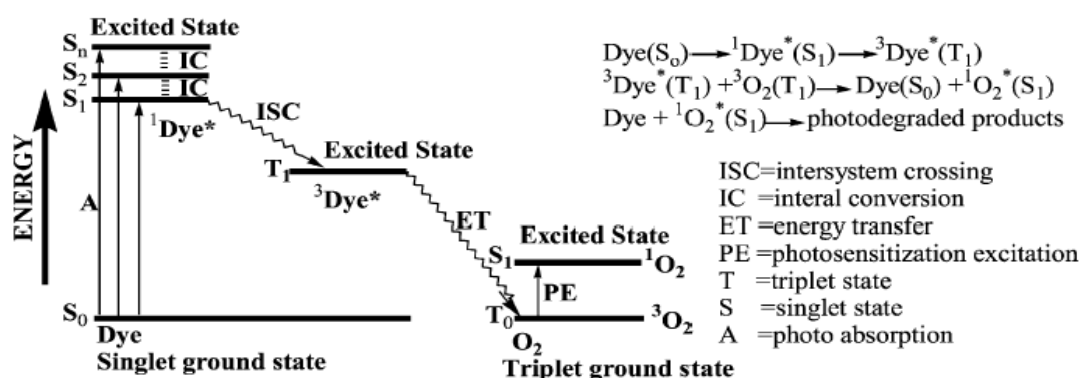


Figure 11 Photolysis mechanism of dye/visible light system (Xie and Yuan, 2003).

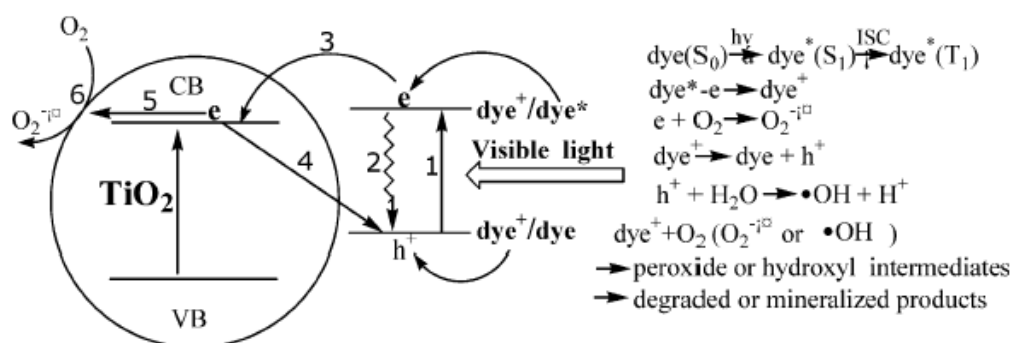


Figure 12 Dye photosensitization mechanism of TiO_2 nanocrystallites.

(Xie and Yuan, 2003)

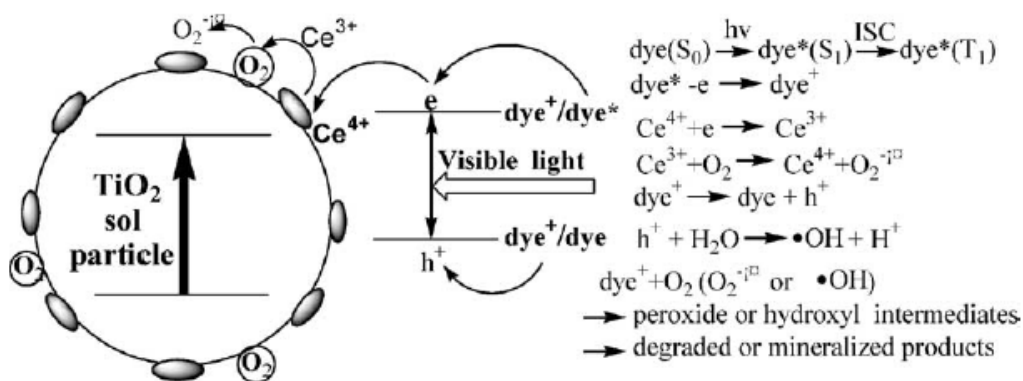


Figure 13 Photosensitized photocatalysis mechanism of Ce^{4+} - TiO_2 sol System.

(Xie and Yuan,2003)

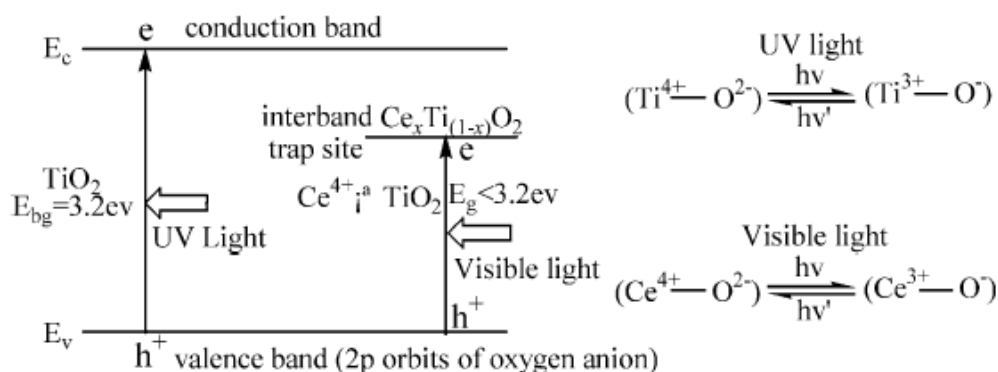


Figure 14 Interband photocatalysis mechanism of Ce^{4+} - TiO_2 nanocrystallites.

(Xie and Yuan,2003)

In the present work, trivalent (Al, B) doped titanium dioxides were prepared by using sol-gel method. In the case of Al-doped TiO_2 , Al dopant was chosen because it has high surface area and good thermal stability. Anderson et al. (1997) prepared mixed oxides of $\text{TiO}_2/\text{Al}_2\text{O}_3$ by sol-gel method and studied the photocatalytic decomposition of salicylic acid. They found that the mixed oxide materials were more efficiency than pure TiO_2 material. Bae et al. (1998) prepared ceramic Al_2O_3 - TiO_2 composite membrane by sol-gel method, the mixed composite exhibited much higher heat resistance than the TiO_2 membrane. Escobar et al. (2000) prepared Al_2O_3 - TiO_2 materials by sol-gel method using different additives (HNO_3 , NH_4OH , and CH_3COOH). The CH_3COOH and NH_4OH additives yielded products with high pore volume and high surface areas than the HNO_3

additive. In the case of B-doped TiO₂, B dopant was chosen because it had not been studied along with TiO₂ before. However, B dopant had been used in diamond (Ekimov et al., 2004), Si (001) wafer (Nishino et al., 1986), carbon nanotube (Charlier et al., 2002), and SiGe alloy (Albenze et al., 2004) in order to improve some of their properties. These synthesized trivalent (Al, B) doped TiO₂ samples were characterized by several techniques such as XRD, BET, TGA, DTA, SEM, TEM, WDXRF, FT-IR, and UV-Vis technique. The photocatalytic degradation of methylene blue (MB) was investigated, employing a UV light source and trivalent (Al, B)-doped TiO₂-based catalysts, and comparing with commercial Degussa P25 TiO₂ catalyst under the same treatments.

1.3 Objectives

- 1.3.1 To prepare undoped TiO₂ and trivalent (Al, B)-doped TiO₂ nanocrystalline by sol-gel method from the hydrolysis and condensation reaction of titanium tetrachloride at low temperature and without calcination.
- 1.3.2 To study the difference in some properties of synthesized undoped TiO₂ and trivalent (Al, B)-doped TiO₂ by sol-gel method.
- 1.3.3 To investigate the photocatalytic activity of MB by these synthesized TiO₂, and compare with commercial Degussa P25 TiO₂ catalyst under the same conditions.